A Decade of Volcanic Construction and Destruction at the Summit of NW Rota-1 Seamount: 2004-2014

Susan R. Schnur[1], William W. Chadwick, Jr.[2], Robert Embley[3], Vicki Ferrini[4], Cornel de Ronde[5], Katharine Cashman[6], Nick Deardorff[7], Susan G. Merle[2], Robert Dziak[3], Joe Haxel[2], and Haru Matsumoto[2]

[1] *College of Earth, Ocean and Atmospheric Sciences, Oregon State University, 104 CEOAS Admin Bldg., Corvallis, OR, USA.*
[2] *Cooperative Institute of Marine Resources Studies, Oregon State University, Newport, Oregon, USA.*
3 NOAA Pacific Marine Environmental Laboratory, Newport, OR, USA
4 Lamont Doherty Earth Observatory, Columbia University, Palisades, NY, USA
5 GNS Science, Lower Hutt, New Zealand
6 School of Earth Sciences, University of Bristol, Bristol, UK
7 Department of Geoscience, Indiana University of Pennsylvania, Indiana, PA, USA

Key Points

1) Repeat bathymetric mapping, ROV observations and hydrophone records document changes in geology and eruptive style at NW Rota-1 Seamount
2) Changes in eruptive activity between 2009 and 2010 impacted the type and distribution of geologic lithofacies at the summit of NW Rota-1
3) Landslides are important agents of change at submarine arc volcanoes and their frequency is controlled by cyclic eruptive activity

Abstract

Arc volcanoes are important to our understanding of submarine volcanism, because at some sites frequent eruptions cause them to grow and collapse on human timescales. This makes it possible to document volcanic processes. Active submarine eruptions have been observed at the summit of NW Rota-1 in the Mariana Arc. We use ROV videography and repeat high-resolution bathymetric surveys to construct geologic maps of the summit of NW Rota-1 in 2009 and 2010, and relate them to the geologic evolution of the summit area over a ten-year period (2004-2014). We find that 2009 and 2010 were characterized by different eruptive styles, which affected the type and distribution of eruptive deposits in the summit. 2009 was characterized by ultra-slow extrusion and auto-brecciation of lava at a single eruptive vent, producing a large cone of blocky lava debris. In 2010, higher energy explosive eruptions occurred at multiple closely-spaced vents, producing a thin blanket of coarse tephra overlying lava flow outcrops. A landslide that occurred between 2009 and 2010 had a major effect on lithofacies distribution by removing the debris cone and other unconsolidated deposits, revealing steep massive flow cliffs. This relatively rapid alternation between construction and destruction forms one end of a seamount growth and mass-wasting spectrum. Intra-plate seamounts, which tend to grow larger than arc volcanoes, experience collapse events that are orders of magnitude larger and also much less frequent than those occurring at subduction zone settings. Our results highlight the interrelated cyclicity of eruptive activity and mass wasting at submarine arc volcanoes.

1. Introduction

The large-scale collapse of submarine volcanoes and ocean islands over time scales of thousands to millions of years has been well-documented [e.g. *Holcomb and Searle*, 1991; *Mitchell*, 2003; *Moore et al.*, 1994]. However, our understanding of both small and large-scale failure processes at active seamounts on time scales of months to years, and the eruptive conditions and deposits that lead to these instabilities is limited. NW Rota-1 is an active seamount in the Mariana volcanic arc in the western Pacific, and one of only two submarine volcanoes in the world where eruptions have been observed during remotely operated vehicle (ROV) dives. This makes it an ideal location to study the interplay between constructive and destructive processes on volcanically active seamounts.

1.1. Previous Work at NW Rota-1

NW Rota-1 is located about 100 km north of the island of Guam (Figure 1a) and was first mapped in detail during a regional bathymetric and water-column survey of the Mariana Arc in 2003 [*Baker et al.*, 2008; *Embley et al.*, 2004; *Resing et al.*, 2009]. The volcano was first visited with an ROV in 2004, at which time it was actively erupting [*Embley et al.*, 2006]. We made ROV observations in 2004, 2006, 2009 and 2010, with additional ROV dives by Japanese investigators in 2005 and 2008. Remarkably, the volcano was observed to be volcanically active on every visit during this time period, but the nature and intensity of the activity as well as the deposits produced changed from year to year. An ROV dive made in 2014 (during expedition RR1413 on R/V *Revelle*) found that the volcano had stopped erupting. The character of the eruptive activity at NW Rota-1 during 2004 and 2006 was described by *Embley et al.* [2006], *Chadwick et al.* [2008a] and *Deardorff et al.* [2011]. Hydrothermal and CO_2 bubble plumes over the volcano and their temporal evolution were described by *Resing et al.* [2007], *Walker et al.* [2008] and *Chadwick et al.* [2014]. In addition to ROV work, in-situ hydrophones have provided records of eruptive strength and duration during 2006 [*Chadwick et al.*, 2008a] and continuously from 2008 to 2010 [*Dziak et al.*, 2012]. One of these hydrophones helped establish the timing of a major landslide event in August 2009 [*Chadwick et al.*, 2012].

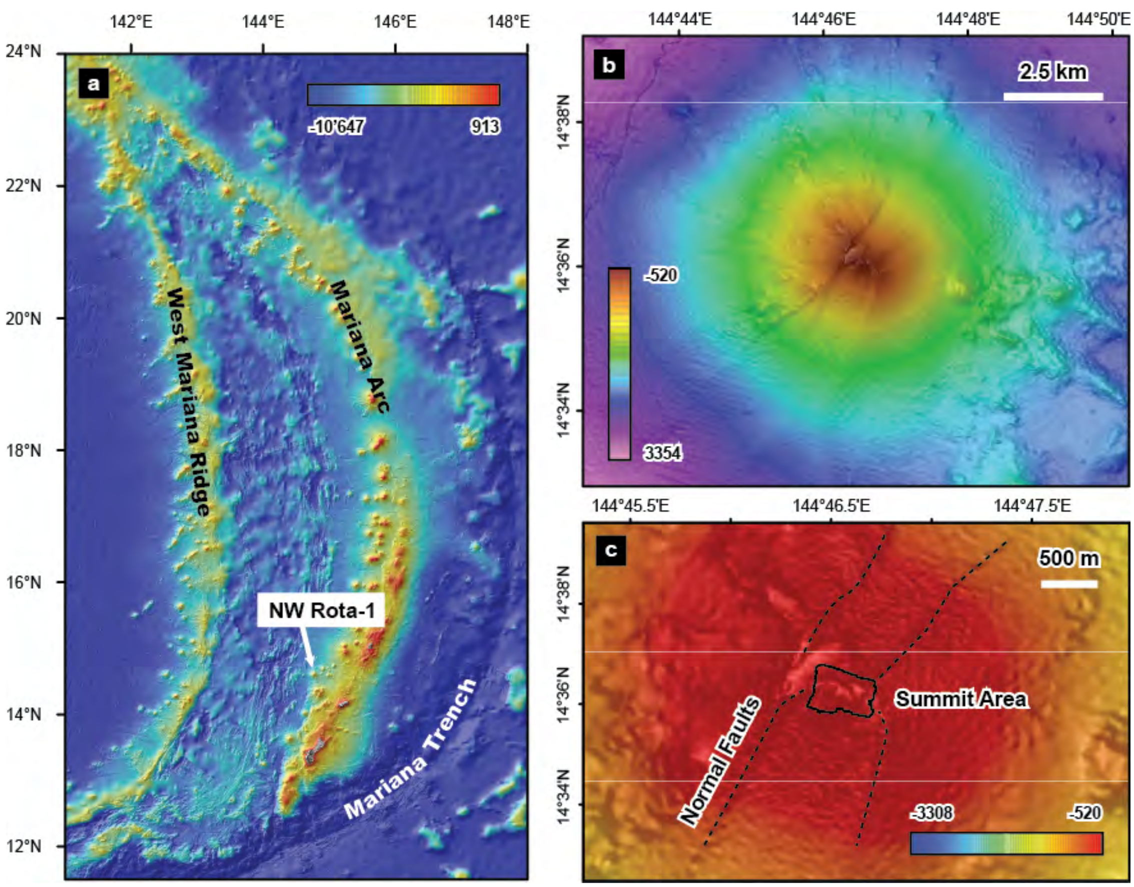

Figure 1. Maps of NW Rota-1 submarine volcano in the Mariana Arc. (a) Regional location, (b) Edifice morphology, (c) Location of the geologically active summit area and surrounding tectonic features.

1.2. New observations from 2009 and 2010

The primary goal of this paper is to document the rapidly changing geology of the summit area of NW Rota-1 by comparing data collected in April 2009 (during expedition TN-232 on *R/V Thompson*) and March 2010 (during expedition KM1005 on *R/V Kilo Moana*) to previous work in 2004 and 2006. We use observations from video recordings and navigation data from ROV dives in order to construct geologic maps of the summit area during 2009 and 2010. We combine the maps with high-resolution bathymetry collected in 2004, 2009, and 2010 to delineate changes in the geomorphology of the summit area as well as the abundance and distribution of volcanic deposits. We highlight the connection between changes in explosive and effusive eruptive activity and the observed eruptive products and how these relate to the recorded hydrophone data. Since the 2010 data provide a post-landslide view of the summit region, these results allow us to explore the factors that determine which deposits are removed and which parts of the seamount resist erosion during large scale failure. Our results provide new insight into the long-term evolution of submarine arc volcanoes.

2. NW Rota-1 Submarine Arc Volcano

NW Rota-1 is one of about 60 submarine volcanoes in the Mariana Arc [*Baker et al.*, 2008; *Lupton et al.*, 2008; *Resing et al.*, 2009], an oceanic island arc located just west of the Pacific-Philippine convergent margin [*Stern et al.*, 2003] (Figure 1a). The edifice is conical, measuring 16 km in diameter at its base and rising almost 2200 m to a summit depth of about 520 m (Figure 1b). The lavas are basaltic to basaltic-andesite in composition [*Tamura et al.*, 2011] and eruptive activity is generally classified as Strombolian, with cyclic eruptions dominated by high gas flux and low magma extrusion rate [*Chadwick et al.*, 2008a]. ROV exploration has focused on an approximately 500 x 600 m region at the summit, encompassing the eruptive vent(s) and surrounding areas of diffuse hydrothermal flow [*Butterfield et al.*, 2011] that support a unique chemosynthetic biological community [*Embley et al.*, 2006; *Hanson et al.*, 2015; *Limén et al.*, 2006; *Meyer and Huber*, 2014; *Sherrin et al.*, 2011]. The summit region is characterized by a NW-SE-trending ridge bounded by a perpendicular set of normal faults (Figure 1c). To the north and south, the edifice falls away in 30° slopes dominated by pebble to cobble-sized pyroclastic debris. The recent eruptive vents are located on the steep south-facing slope, about 30-40 m below the summit, such that eruptive products are primarily funneled down the south flank. During 2004-2009, one eruptive vent named Brimstone was active, but in 2010 (after the landslide) five closely-spaced vents displayed eruptive activity (including Brimstone).

3. Methods

3.1. Bathymetry and Navigation

We use high-resolution (2 m) bathymetry of the summit area of NW Rota-1 collected in 2004, 2009 and 2010 (Figure 2) to make quantitative comparisons of changes in depth between these years. The 2004 survey was collected by the *ROPOS* ROV with an Imagenex scanning sonar (675 kHz), and was processed as described in *Chadwick et al.* [2001]. The 2009 and 2010 surveys were made by the *JASON* ROV using an SM2000 multibeam sonar (200 kHz), and were processed following the methods of *Ferrini et al.* [2008]. The 2004 bathymetry is derived from sparser data (due to the Imagenex being a single-beam scanning sonar). In each survey, the seafloor depth soundings are a geometric combination of the ROV depth and the acoustic range from the ROV to the bottom, and are accurate to ± 20 cm. More importantly, the horizontal position of the depth soundings is dependent on the ROV navigation, which is variable and typically ± 1 m in relative position (based on a Doppler sonar on the ROV), but up to ± 10-20 m in absolute position (based on acoustic navigation from the ship to the ROV).

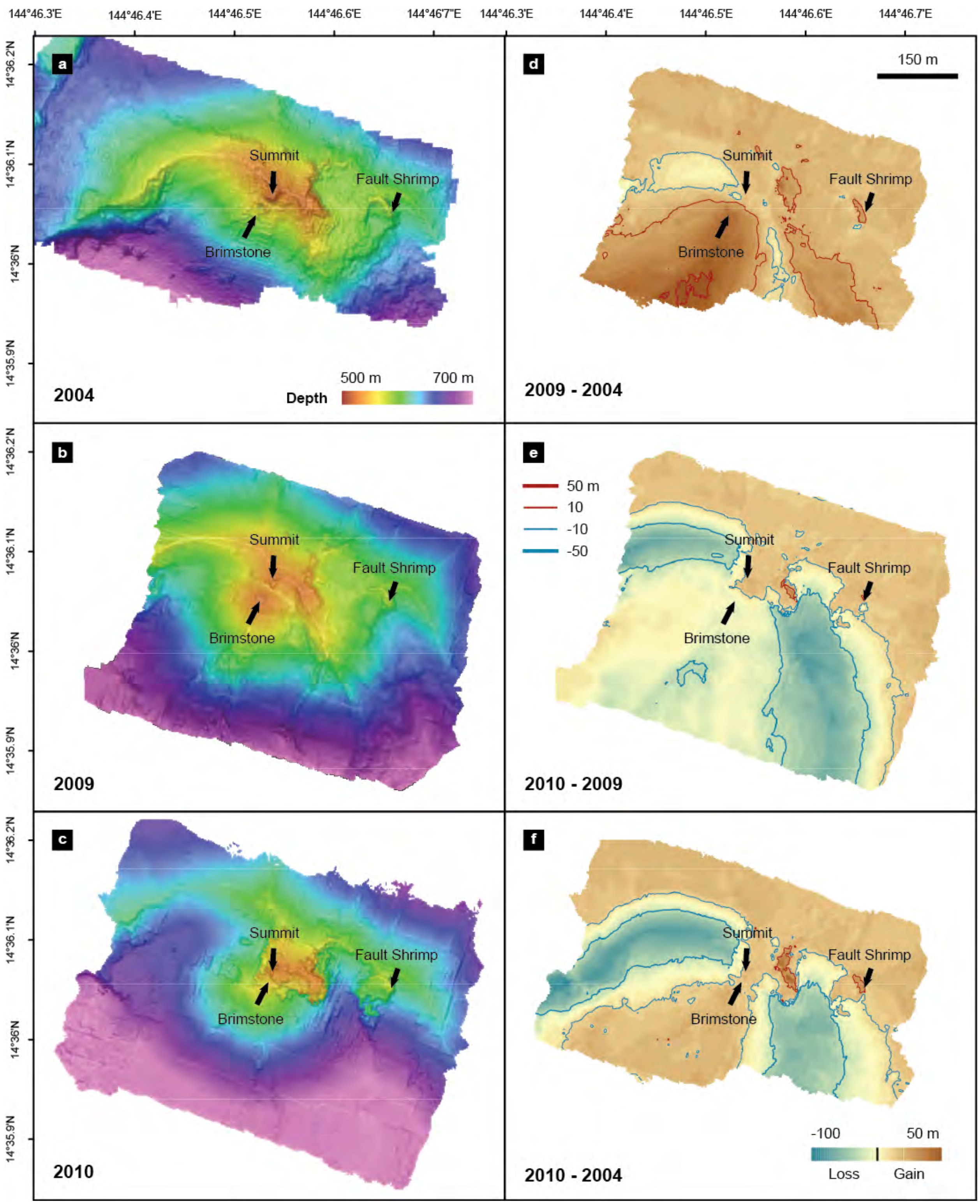

Figure 2. Left: Maps of high-resolution bathymetry derived from surveys conducted in (a) 2004, (b) 2009, and (c) 2010. The maps highlight changes in morphology due to constructive and destructive processes. Locations of Brimstone eruptive vent, the Summit Ridge, and Fault Shrimp hydrothermal site are shown. Right: Depth changes determined by repeat high-resolution

multibeam surveys in 2004, 2009 and 2010. Contour lines indicate areas of greatest change. Most minor depth changes (<10-20 m) are a result of uncertainty in multibeam georeferencing (ROV navigation). Major changes are due to volcanic construction between 2004 and 2009 (d), and landslide activity between 2009 and 2010 (e). Locations of Brimstone, Summit Ridge, and Fault Shrimp are shown for reference.

The absolute navigation for the 2004 and 2010 surveys was derived from ultra-short baseline (USBL) navigation systems, whereas in 2009 we attempted to use a long-baseline (LBL) transponder system with poor results. Due to the high currents at the shallow depths of the summit area (500-600 m) and the 200 m tethers used on the transponders, the repeatability of the LBL navigation was found to be so poor (40-50 m) that it was not useful for our purposes. In 2009, we therefore relied solely on the ROV's Doppler sonar navigation (Doppler Velocity Log or DVL), referenced to previously known sites or seafloor marker positions. The repeatability of the 2009 DVL-only navigation at NW Rota-1 is estimated to be 10-20 m, whereas the 2004 and 2010 USBL navigation repeatability is estimated at 5-10 m.

Each high-resolution bathymetric data set was edited to remove outliers and gridded at a resolution of 2 m. The earlier two surveys were shifted to best match the 2010 survey; the 2004 bathymetric grid was shifted 14 m North and 10 m East, whereas the 2009 grid was shifted 10 m South and 10 m East. No vertical shifts (in depth) were made to the surveys. The bathymetric surveys in 2004, 2009, and 2010 covered areas of 0.333 km^2, 0.299 km^2 and 0.339 km^2 respectively, of which 0.201 km^2 was shared by all three surveys (Figure 3). Once geographically co-registered, the grids could then be subtracted from one another to quantify depth differences between the surveys. These results were used to highlight areas where constructive volcanism had added material to the summit (positive depth changes) or where mass wasting processes had removed material from the summit (negative depth changes) between the surveys.

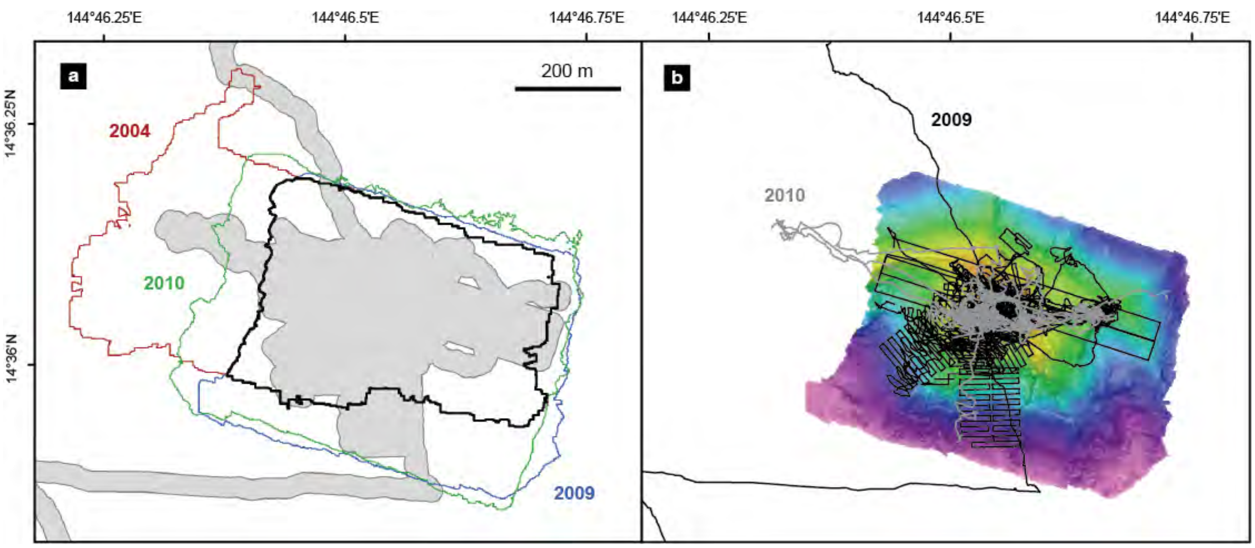

Figure 3. Overview of ROV dive tracks and extent of geologic mapping in the summit area of NW Rota-1. (a) Grey outline shows a 20 m buffer placed around the combined dive tracks of 2009 and 2010, representing the total coverage of ROV observations. This region includes almost the entire area of overlap (black outline) between bathymetry collected in 2004, 2009 and 2010. (b) Dive tracks from 2010 and 2009, indicating which areas of the summit received the densest coverage of exploration.

3.2. Geologic Mapping and Lithologic Facies

The *JASON* ROV conducted 17 dives at NW Rota-1 in 2009 and 10 dives in 2010. Dive objectives included hydrothermal fluid sampling and observation of fauna at hydrothermal upflow zones as well as visual observations of the geology, changes in eruptive activity, and the distribution of recent eruptive deposits. These operations provided coverage dense enough to observe multiple contacts between different lithofacies zones across the summit area (Figure 3). We used *JASON* ROV dive navigation to geo-reference lithofacies occurrences and unit contacts observed during the dives. These contacts, along with terrain changes observed in the high-resolution bathymetry, were used to manually define unit boundaries and create geologic maps of the summit area in 2009 and 2010.

For our geologic mapping, we established a set of eleven lithofacies that encompasses the wide range of geologic deposits observed in 2009 and 2010 (Figures 4 and 5). Our choice of lithofacies distinguishes between the youngest eruptive products and older deposits, explosive versus effusive eruptive products, and consolidated versus unconsolidated materials. The relative age of deposits was determined based on superposition, degree of erosion, alteration and cementation, as well as mantling by tephra and sulfur. Proximity to the active vent, comparison to previous ROV observations, and degree of preservation from year to year also provided clues for estimating the relative ages of the deposits. Clast size was estimated based on a pair of lasers on the ROV spaced 10 cm apart.

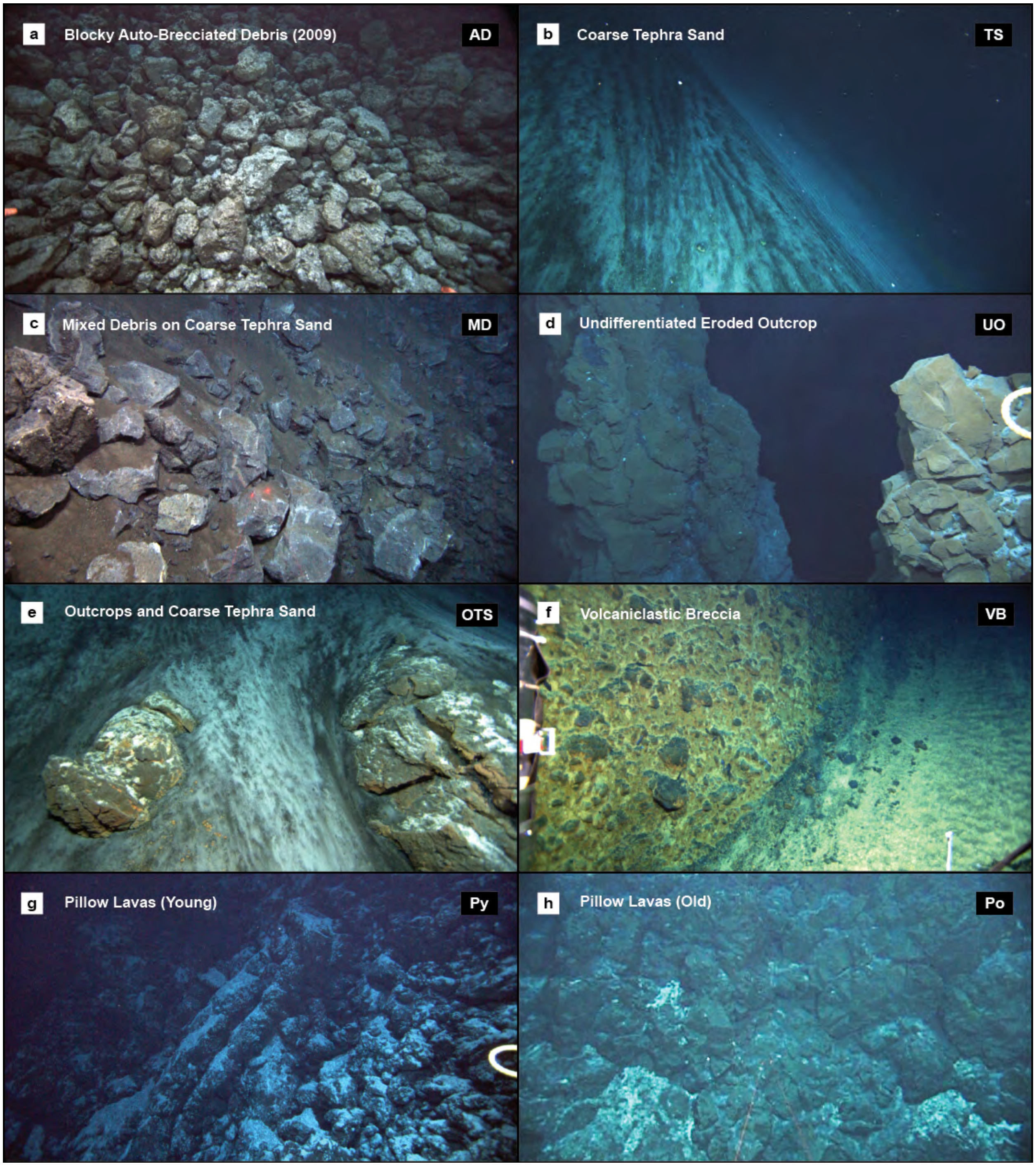
a
Blocky Auto-Brecciated Debris (2009)
AD
b
Coarse Tephra Sand
TS
c
Mixed Debris on Coarse Tephra Sand
MD
d
Undifferentiated Eroded Outcrop
UO
e
Outcrops and Coarse Tephra Sand
OTS
f
Volcaniclastic Breccia
VB
g
Pillow Lavas (Young)
Py
h
Pillow Lavas (Old)
Po

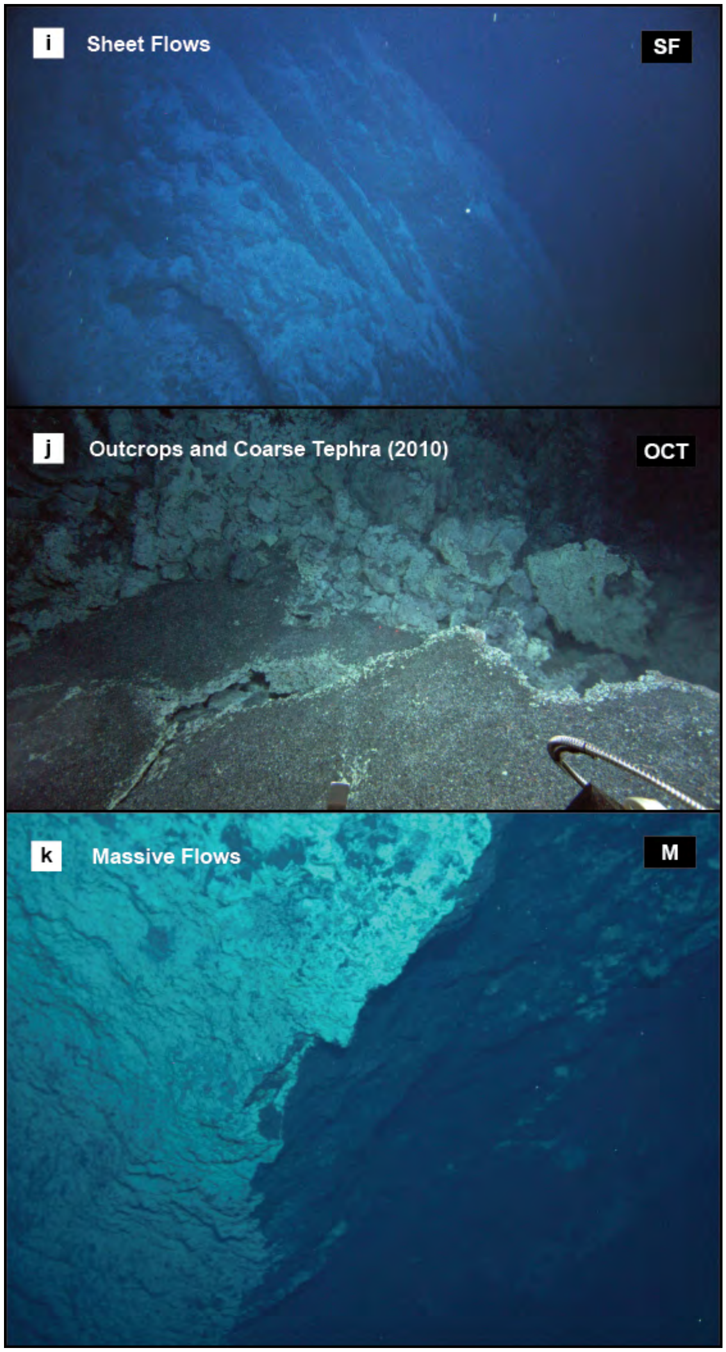

Figure 4. Photos of typical appearances of lithofacies used to construct geologic maps. (a) Blocky Auto-Brecciated Debris (see also Video 1), (b) Coarse Tephra Sand, (c) Mixed Debris on Coarse Tephra Sand, (d) Undifferentiated Eroded Outcrop, (e) Outcrops and Coarse Tephra Sand, (f) Volcanic Breccia, (g) Young Pillow Lavas, (h) Old Pillow Lavas, (i) Sheet Flows, (j) Outcrops and Tephra Gravel, (k) Massive Flows. Facies IDs shown on each image match the legend included in the geologic maps (Figure 9). The location where each picture was captured is shown in Figure 5.

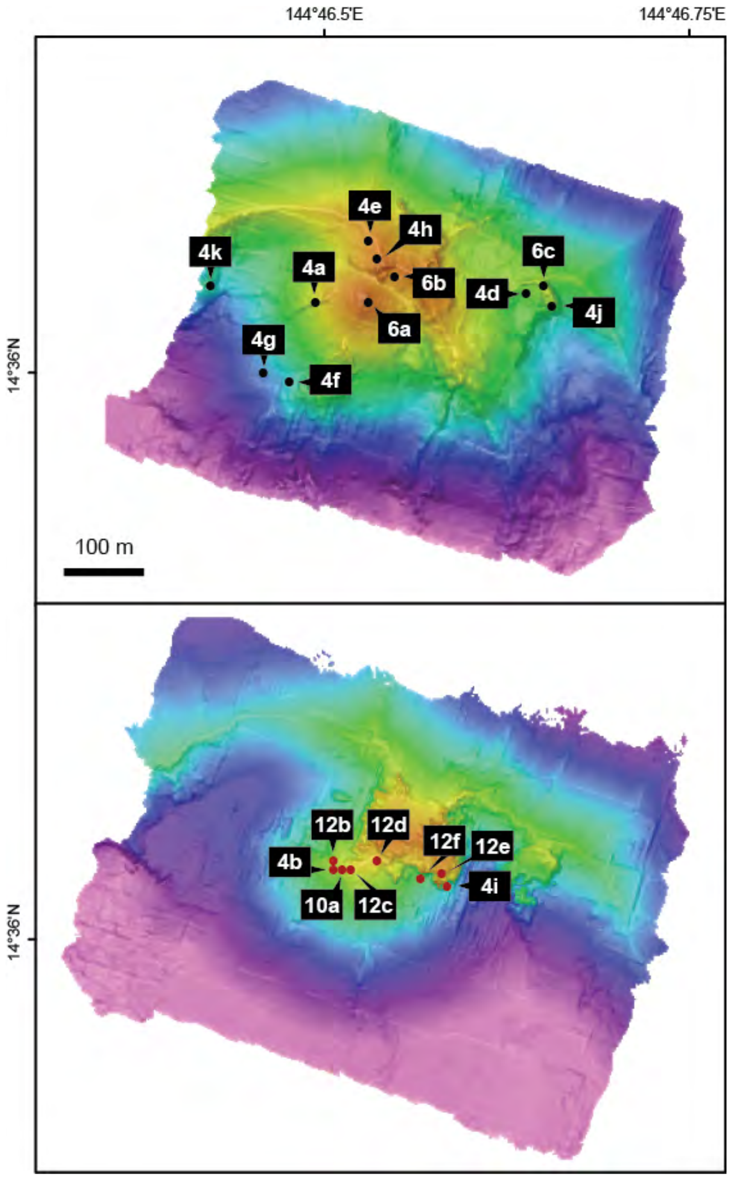

Figure 5. Locations of photos shown in Figures 4, 6 and 11, shown overlaid on multibeam bathymetry for 2009 and 2010.

3.3. Hydroacoustic Observations

Four hydrophone records are available over the 2009-2010 time period. Long-term acoustic recordings were made continuously by two deployments of a moored hydrophone, the first from April 2008 to February 2009, ending a month before the 2009 ROV expedition, and the second from February 2009 to April 2010, including during most of the 2010 ROV expedition. Also available are short-term sound recordings made by portable "B-Probe" hydrophones deployed at the summit during both the 2009 and 2010 ROV expeditions (~30 m north of Brimstone Vent). B-Probe hydrophones were deployed three times each in 2009 and 2010, providing near-vent acoustic records in both years. The hydrophone data provide the opportunity to directly relate acoustic time-series data with ROV video observations, allowing us to quantify the relative amplitudes of eruptive activity and to observe changes in the character of this activity over time. The moored hydrophone in 2008-2009 was located ~150 m NE of Brimstone vent [*Dziak et al.*, 2012] and the 2009-2010 deployment was located ~400 m to the WNW of the vent [*Chadwick et al.*, 2012].

4. Observations in 2009

4.1. High-Resolution Multibeam Bathymetry

The summit landscape in 2009 was dominated by a cone of blocky auto-brecciated lava debris centered at the eruptive vent (Figures 2b, 6a and Video 1). This cone was not present during previous ROV dives in 2004 and 2006 (Figure 2a). The new circular cone was ~300 m in diameter and 40 m high, with a summit depth of ~520 m and generally uniform slopes of ~30-35° (Table 1). The cone had built up over the Brimstone eruptive vent south of and adjacent to the sharp NW-SE-trending summit ridge which has a crest at 517 m. Multiple satellite ridgelines radiate outwards from the summit ridge (Figures 2b and 6b), generally trending NW-SE or NE-SW. The Fault Shrimp area is a secondary elevated ridge to the east of the summit at about 565-575 m depth that hosts diffuse hydrothermal venting (Figures 2b and 6c). Note that in Table 1 the only significant change in the depth of key features is at Brimstone. All other features remain at the same depth and average slopes also remain at the angle of repose (~30°). Also evident in the bathymetry (and confirmed by visual observations) is a fan-shaped area of pillow lavas on the south flank of the debris cone that is slightly elevated and partially overlain by the blocky lava debris (Figure 2b and 4g). This area of pillow lavas was not present in 2004 and 2006, indicating that the pillows must have been emplaced during an earlier higher eruption rate phase of cone construction prior to the formation of the rest of the blocky lava cone in 2009, which reflects a lower eruption rate.

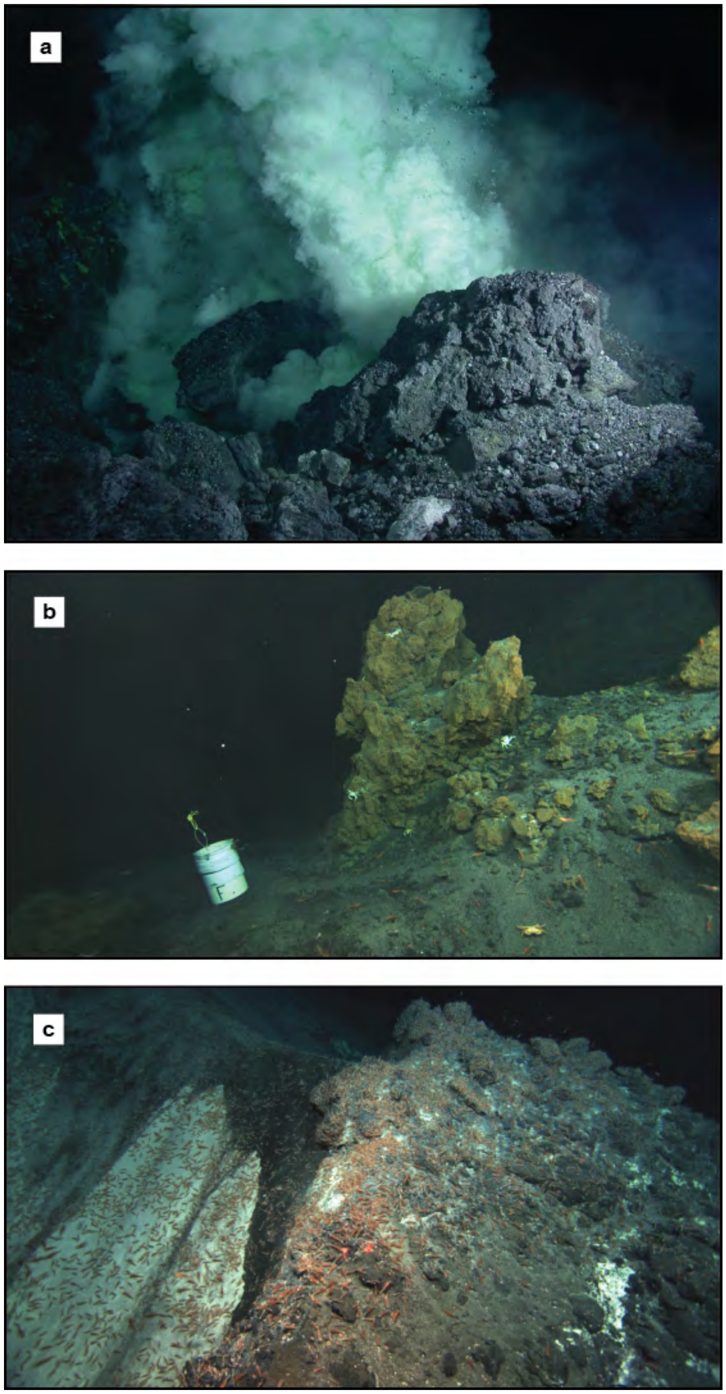

Figure 6. Key locations in 2009. (a) Brimstone vent and debris cone, (b) Outcrops and coarse tephra sand at the summit ridge in 2009, (c) Volcanic breccia at the edge of Fault Shrimp.

Table 1. Depths of key features and slope statistics determined from high-resolution bathymetric surveys conducted in 2004, 2009 and 2010.

	Depths of Key Features [m]			Slope Statistics [º][1]		
	Brimstone Vent	Summit Ridge	Fault Shrimp	Mean	Standard Deviation	Max
2004	560	517	565	32	14	83
2009	520	517	565	30	10	82
2010	550	517	565	31	12	87

[1] Slope values were calculated from a projected version (UTM 55N) of the high resolution bathymetry. The median and mode of the slope values are similar to the mean and are therefore not shown here.

4.2. Depth Changes

Depth changes between the high-resolution multibeam surveys can be quantified by subtracting one survey from another (Figure 2). Compared to the previous multibeam sonar survey in 2004 (and ROV observations in 2006), the bathymetry in 2009 showed major depth decreases due to the addition of erupted material at and downslope from the Brimstone vent area. The eruptive vent was 40 m shallower in 2009 than in 2004 and 2006 (Table 1), mainly due to the growth of the blocky auto-brecciated lava cone. Because the cone was built on the steep south flank of the volcano, 2004-2009 depth changes at the cone merged with a tongue of depth decrease (i.e. the addition of material) that extended downslope from the eruptive vent, due to the remobilizing of debris down the slope as the cone grew (Figure 2d). The largest depth decrease was observed at the foot of the pillow lavas downslope from the cone. Other apparent depth changes beyond the new cone are < ± 20 m and are probably due to navigation errors between the 2004 and 2009 surveys combined with steep slopes. Overall the addition of material to the summit area between 2004 and 2009 (within the area of high-resolution multibeam coverage), amounted to a volume of about 1.41×10^6 m^3 (Table 2). However, this volume is only the upper part of the larger tongue of material that accumulated on the upper flanks between 2003 and 2009. The whole tongue extended 4 km downslope from the vent and totaled 34 × 10^6 m^3, as documented by ship-based multibeam surveys [*Chadwick et al.*, 2012].

Table 2. Summary of depth and volume changes between years from within the area of overlap between all three of the high-resolution multibeam sonar surveys.

Time Period		Depth Change [m][1]				Volume Change [10^6 m^3]		
		Shallowing (+)		Deepening (-)		Gross		Net
From	To	Mean	Max	Mean	Max	Gain	Loss	
2004	2009	13.6	59.7	-5.1	-41.0	1.77	0.36	1.41
2004	2010	3.7	38.4	-27.5	-89.2	0.19	4.10	-3.91
2009	2010	2.6	37.0	-28.4	-93.4	0.03	5.38	-5.36

[1] Depth differences are calculated by subtracting the initial year from the comparison year (e.g. 2009 - 2004). A positive difference therefore represents an increase in height of the seafloor (a shallowing) whereas a negative difference indicates a drop in the height of the seafloor (a deepening).

4.3. Eruptive Style

During the 2009 ROV dives, only a single eruptive vent was active (Brimstone), as had been the case in 2004 and 2006. ROV observations of the vent area were made during 17 separate visits over a period of 12 days, each lasting from 15 minutes to 4.5 hours. The eruptive activity at Brimstone vent, which measured 1-2 m across, was characterized in 2009 by extremely slow extrusion of lava accompanied by cyclic passive-to-vigorous degassing (Video 2). This included variable emission of a white sulfur-rich particle plume and bubbles of CO_2 sometimes accompanied by tephra. No incandescent lava was observed in 2009, in contrast to 2006 when the eruptive style was more explosive and the eruption rate was distinctly higher [*Chadwick et al.*, 2008a]. The ultra-slow lava extrusion in 2009 could only be confirmed by long observations at the vent and especially time-lapse video sequences. This activity also produced distinctive eruptive products that were different from previous years. We believe this style of submarine eruption has never been observed at a submarine volcano before (including previous visits to NW Rota-1), and that it represents the low-end of the spectrum of eruptive rates at arc seamounts.

The slow extrusion of lava in 2009 was characterized by the gradual appearance of blocks and spines of lava in the midst of the center of the eruptive vent, often shrouded by sulfur-rich particle plumes. These lava spines grew slowly upwards, eventually tilted outwards, and fell to the side of the vent. Several long (30-60 minute) periods of visual observation at the vent could be made into time-lapse movies, allowing us to calculate that the lava spines moved at rates of about 1-6 m/hour during this slow extrusion process (Figure 7 and Videos 2-4). From the rate of movement and the size of each spine, we estimate that the eruption rate during these periods was on the order of 0.2-7.5 m^3/hr, about 1-2 orders of magnitude lower than in 2006 [*Chadwick et al.*, 2008a].

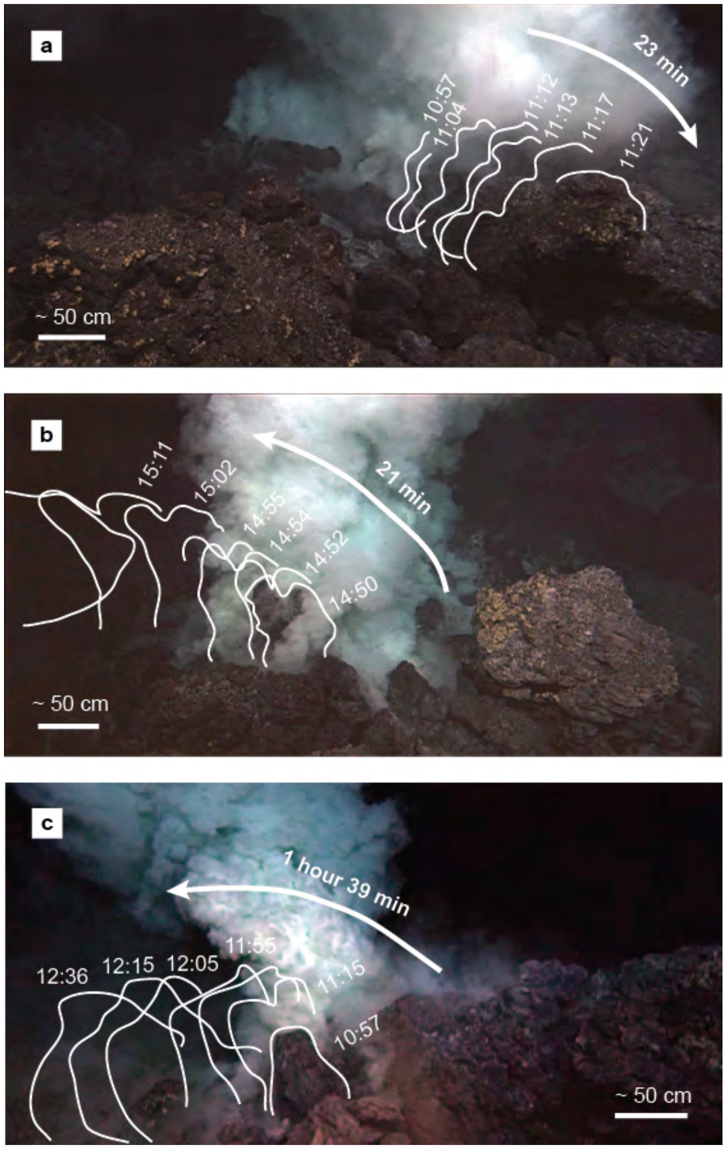

Figure 7. Time-lapse reconstruction of ultra-slow lava extrusion at Brimstone vent in 2009. Examples are shown from three different dives, with white lines indicating the manually-traced outlines of slowly moving lava blocks (a,c) and spines (b) as well as time stamps for each observation. Distance calculations for diagram (a) are corrected for the 45° degree viewing angle of the camera. See also Videos 2-4.

Because of this ultra-slow rate of extrusion and rapid cooling by seawater, the lava emerging from the vent was gradually broken into smaller pieces within meters of the vent, as more lava was forced up behind it. The lava being actively extruded from the vent at any one time would effectively break up the previously extruded (and now cooled) lava ahead of it. The slow extrusion would also cause repeated shaking and jostling of the newly erupted material in the vent area as the lava blocks and spines were forced upwards within the vent (Video 4). ROV observations witnessed multiple small avalanches of blocky material cascading down the sides of the debris cone as newer lava from the vent shoved older lava over the brink (Video 3). Over time this slow extrusion process generated the blocky debris cone that characterized the summit in 2009.

The slow extrusion process was observed to be cyclic on a time scale of minutes, both from ROV observations at the vent and from hydrophone recordings. *Chadwick et al.* [2008a] observed a strong periodicity to the eruptive activity at NW Rota-1 in 2006, with explosive bursts lasting several minutes, separated by shorter pauses of relative quiescence. This periodicity was explained with a model in which magmatic gas becomes segregated in the conduit, and each eruptive burst begins with the arrival of a gas pocket at the eruptive vent. The pauses between bursts permitted cold seawater to penetrate below the seafloor and form a quenched lava cap at the top of the conduit, which temporarily sealed the vent but was subsequently lifted and eventually blown apart by the next gas burst.

The cyclic slow extrusion observed in 2009 likely represents a very similar process to that proposed for the activity in 2006 except at a much lower eruption rate. During the 2009 ROV dives, when fresh lava was actively emerging from the vent, degassing became much more vigorous. Visually, this included the plume becoming more yellow as sulfur was rapidly released, and the sudden appearance of abundant CO_2 bubbles. During vigorous degassing, flurries of tephra were observed in the plume , most of which were deposited close to the vent. The tephra was generally small (< 1 cm), and likely represents remobilization of fragmental material already present at the vent. Much of this tephra is also likely a result of quench granulation, and does not represent juvenile fragments [*Deardorff et al.*, 2011]. These cyclic bursts built rapidly and ended abruptly, as reflected in the hydrophone data (see below). During the pauses, active extrusion stopped, the sulfur-rich particle plume would become more passive (exhibiting a less roiling nature) and return to a whiter color, and the emission of CO_2 bubbles would stop (Video 5).

4.4. Hydrophone Observations

The hydrophone data recorded at NW Rota-1 can be used to show temporal variations in the strength of the eruptive activity, and to put the 2009 and 2010 ROV observations into a longer-term quantitative context. Additionally, the hydrophone records help to distinguish explosive eruptive activity from passive degassing when combined with ROV visual observations at the vents [*Chadwick et al.*, 2014]. Both the long-term moored hydrophones and short-term portable hydrophone data show the distinct cyclicity of the eruptive activity at NW Rota-1, with a wide range of signal amplitudes over time. The 2008-2009 moored hydrophone data [*Dziak et al.*, 2012] shows a major change in amplitude between February 2008, November 2008 and January 2009 (Figure 8a). At the start of the record in February 2008, the acoustic amplitudes were consistently high (Figure 8b), but became more variable towards the end of the year (Figure 8c). By January 2009, prior to the 2009 expedition, acoustic amplitudes had lowered significantly (Figure 8d). Regardless, the cyclicity of the eruptive activity was maintained throughout this large change in amplitude.

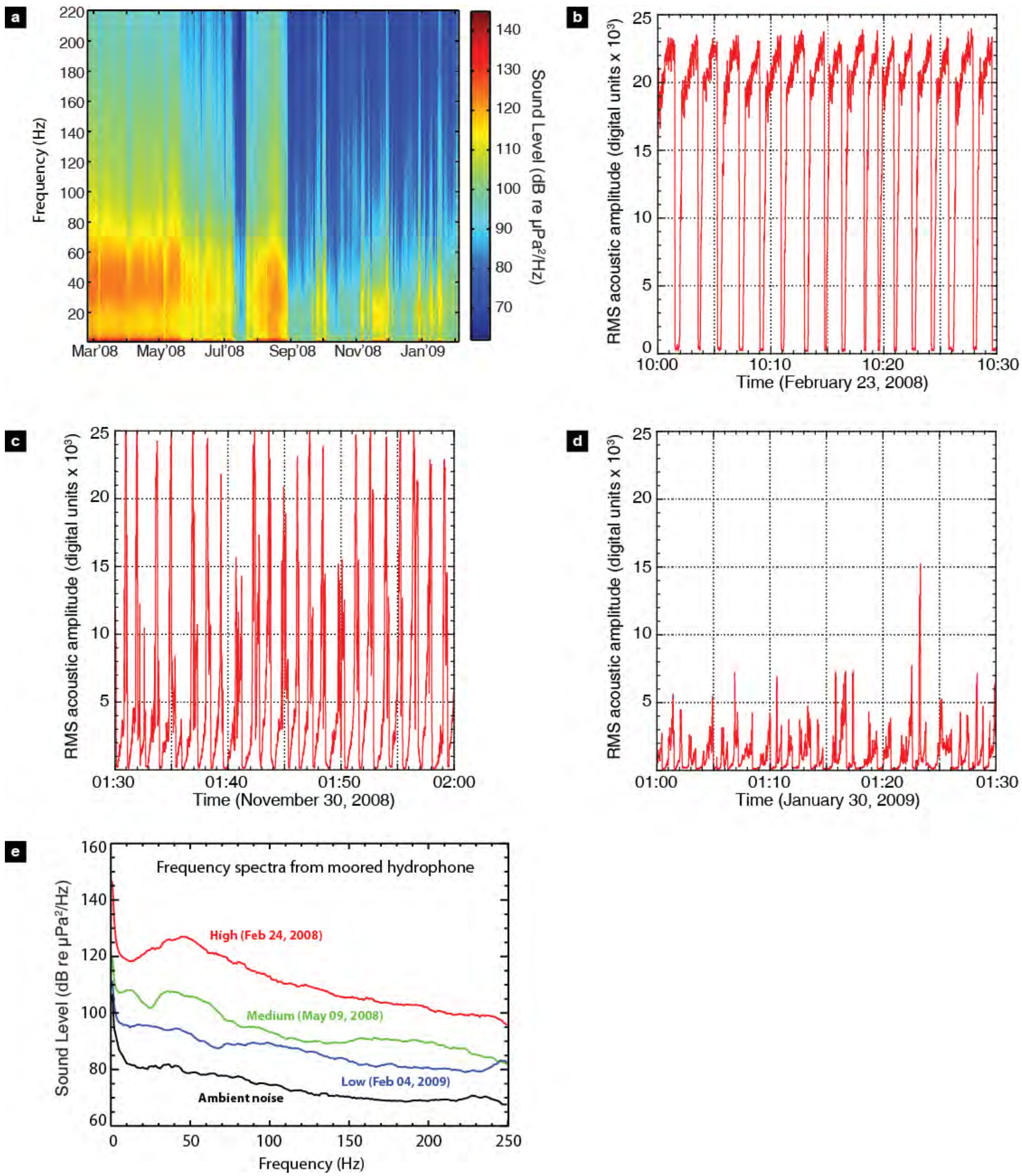

Figure 8. Moored hydrophone data recorded at NW Rota-1 from February 2008 to February 2009. (a) A year-long, daily-average spectrogram showing sound amplitude (colors) in decibels (relative to $\mu Pa^2/Hz$) as a function of frequency versus time. Note first half of the record has much higher sound amplitudes than the second half, indicative of higher levels of eruptive activity (after *Dziak et al.,* [2012]). (b-d) Plots of RMS acoustic amplitude (in digital units, averaged every second) measured by moored hydrophone over 30-minute time intervals,

showing similar cyclicity of eruptive periods and pauses throughout the year, but with varying amplitude. (e) Frequency power spectral density curves comparing relative amplitudes of acoustic signals throughout the year in decibels. Each curve is 10-20 dB (or roughly 5-10 times) louder than the one below. All plots corrected for instrument response, but not for distance from vent (~150 m for all curves).

The acoustic amplitude varied over 10s of minutes and the eruptive activity in February 2008 had very distinct high-amplitude eruptive periods divided by short low-amplitude pauses (Figure 8b). These periods leaped from a baseline level in a matter of seconds then grew more slowly to peak amplitude before dropping abruptly. The eruptive periods ranged in duration from about 80 to 100 seconds. The pauses between eruptive periods were very short, ranging in duration from 10-20 seconds. A similar periodicity was observed during the moderate amplitude activity in November 2008 (Figure 8c), and the much lower amplitude activity in January 2009 (Figure 8d). At that time the eruptive periods lasted about 30-90 seconds, and were divided by pauses of about 10-30 seconds.

The acoustic amplitudes recorded early in 2008 at NW Rota-1 were much higher than those recorded during previous ROV visits in 2006, and those in early 2009 were much lower (Figure 8e). Because acoustic amplitude has previously been shown to closely reflect the intensity of eruptive activity [*Chadwick et al.*, 2008a, 2012], we interpret that high acoustic amplitudes reflect relatively high eruption rates, and that the young pillow lavas observed at the southern-base of the debris cone in 2009 were emplaced during the vigorous eruptive period in early 2008. Similarly, we interpret from the hydrophone record that the rate of eruptive output transitioned to a much lower rate during late 2008 and early 2009, and that the eruptive style shifted to ultra-slow lava extrusion as we observed during the April 2009 ROV dives. This is consistent with the observation that the young pillow lavas are overlain by the blocky auto-brecciated debris generated by slow extrusion at the vent.

4.5. Eruptive Deposits and 2009 Geologic Map

A geologic map of the summit of NW Rota-1 in 2009 is presented in Figure 9a, and the percentage abundance of each facies is listed in Table 3.

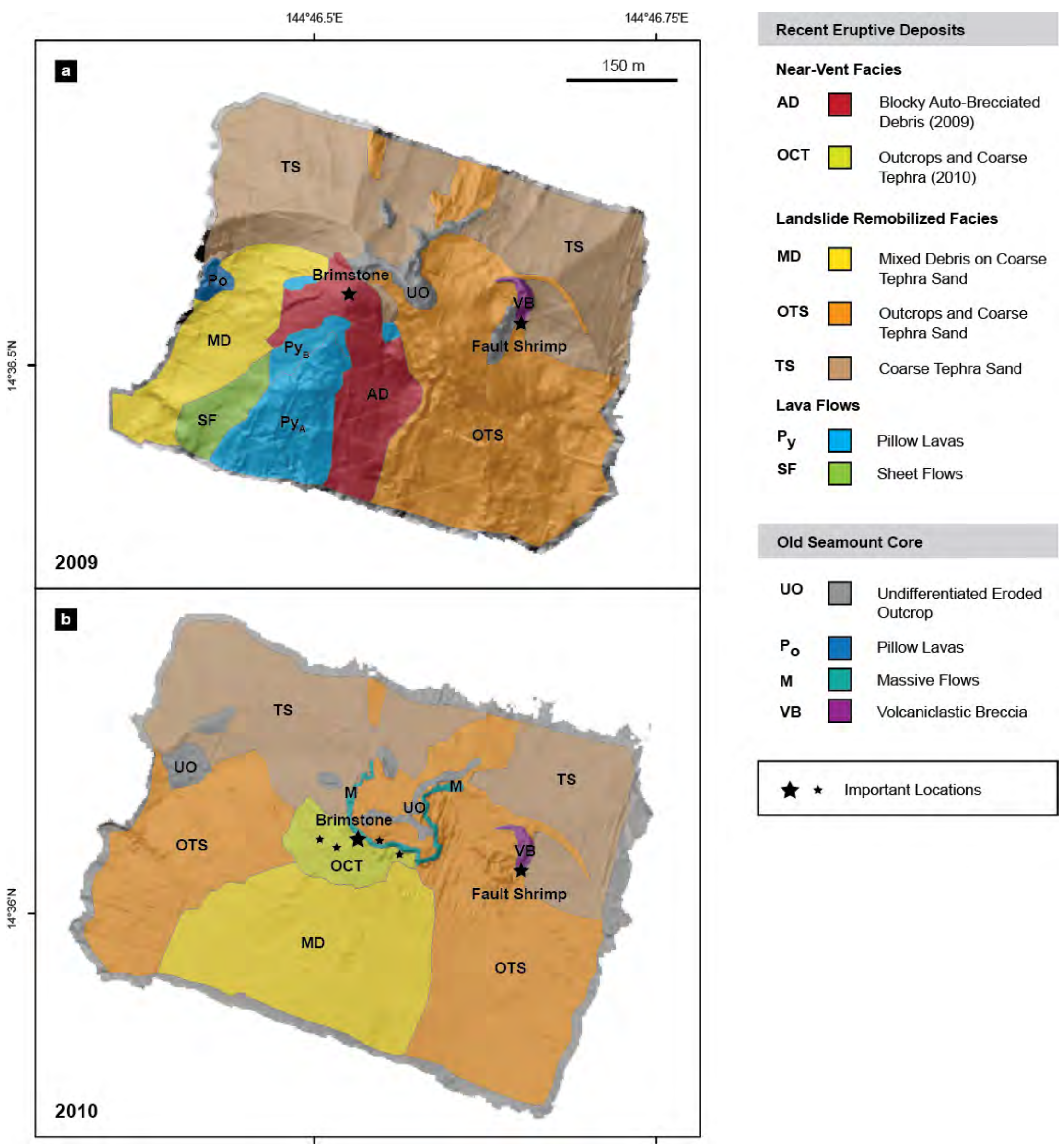

Figure 9. Geologic maps of the summit of NW-Rota-1 in (a) 2009 and (b) 2010. Facies abbreviations are shown in the legend. The locations of Brimstone and other eruptive vents are shown for reference. The five vents observed in 2010 are indicated with stars. From west to east they are Phantom, Sulfur, Brimstone, Styx and Charon. Photographs of the vents and their characteristic eruptive styles are shown in Figure 11.

Table 3. Percentage of summit area covered by each geologic facies.

	2009		**2010**	
	Area [m^2][1]	**Percent [%][2]**	**Area [m^2]**	**Percent [%]**
AD	27469	10	-	-
OCT	-	-	10940	4
MD	28492	10	62405	21
OTS	89900	33	129972	43
TS	87187	32	85435	29
Py	24913	9	-	-
SF	7855	3	-	-
UO	7623	3	7359	3
Po	1807	1	-	-
M	-	-	2734	1
VB	1263	1	1263	< 1

[1] Facies coverage is reported as horizontal area.
[2] Coverage is divided by the total area mapped, not the total area of high-resolution sonar coverage.

In both 2009 and 2010, the vent area was dominated by a different lithofacies characteristic of that year. These near-vent deposits represent the most recent eruptive products in each year, and therefore the most recent style of eruptive activity. The predominant near-vent lithofacies in 2009 was *Blocky Auto-Brecciated Debris (AD)* (Figure 4a). This unconsolidated coarse fragmental debris is generated by the crumbling of lava slowly extruded at the vent (i.e. autoclastic material). Although the process that generates this debris can be classified as effusive, the rapid cooling and crumbling of the slowly-extruded material results in a fragmental deposit that looks like talus but is actually a primary deposit. This lithology consists of pebble to boulder-sized blocky debris forming piles of generally uniform clast size distribution, with most clasts measuring about 20 cm in diameter, although in some cases ranging from 5-160 cm. Clasts are generally sub-angular to very angular, with angularity and size increasing roughly with proximity to the vent, due partly to the low slopes (~ 5-10°) within a few meters directly surrounding the vent. These deposits formed a broad cone surrounding the active vent and comprised about 10% of the mapped area.

A very abundant lithology in both 2009 (32%) and 2010 (29%) was fine to coarse (≤ 1 mm) tephra sand forming smooth, steep slopes close to the angle of repose *(Coarse Tephra Sand, TS)* (Figure 4b). These slopes varied in color from white to almost completely black, depending on how much particulate sulfur had been deposited, and the degree of sulfur cementation and ferro-manganese encrustation following deposition. Sulfur dioxide (SO_2) is an important and abundant component of the magmatic gas output of NW-Rota [*Butterfield et al.*, 2011]. When SO_2 mixes with seawater it produces tiny globules of sulfur which fall out of the eruptive plume, forming deposits with a mix of tephra and sulfur [*Deardorff et al.*, 2011]. It is also likely that sulfur is deposited in the shallow subsurface in areas where hydrothermal fluids vent diffusely through cracks and near-surface sediments. After it is deposited, this particulate sulfur can be remelted and remobilized by hydrothermal heat from below, forming sulfurous crusts and agglomerations with coarse tephra sand, likely providing minor consolidation of otherwise unstable slopes. Older slopes showed a distinct cm-thick sulfur-cemented surface layer that appeared to play a role in inhibiting slope failure.

A variant of these two facies is pebble to boulder-sized (5 to 80 cm) blocky debris sparsely distributed on an underlying tephra slope *(Mixed Debris on Coarse Tephra Sand, MD)* (Figure 4c). This facies was relatively uncommon (10%) and was most likely a result of topographic controls on debris distribution surrounding the active vents. The debris from the vent cone remained abundant on the upper flanks of the summit area, but transitioned gradationally into mixed debris on coarse tephra sand at about 800 m depth. The lower south flank of NW Rota-1 was dominated by this latter facies.

Parts of the old seamount core in both years consisted of outcrops so eroded it was no longer possible to identify the primary lava flow morphology, in which case they are classified as *Undifferentiated Eroded Outcrop (UO)* (Figure 4d). The summit ridge was characterized by these rocky outcrops 2-3 m high at its crest, separated by areas of coarse tephra sand that draped the summit area. The facies *Outcrops and Coarse Tephra Sand (OTS)* (Figure 4e) occurred where tephra sand formed only a thin blanket over older lava flows, and it was the most abundant facies in 2009 (33%). This facies was often found along ridgelines where outcrops only intermittently rose above the surrounding coarse tephra sand. This tephra sand is interpreted to have been deposited from past vigorous explosive activity. Several satellite ridge lines were similarly composed of isolated heavily sulfur-encrusted outcrops, some of which appeared to be weakly cemented older breccias. The area north of the summit ridge was covered predominantly by coarse tephra sand. The area between Fault Shrimp, a small, 40 m-long ridge located about 180 m east of Brimstone vent (Figure 6c), and the summit ridge was also mostly covered in coarse tephra sand.

The valley between the debris cone and the summit ridge (see Figure 2b) consisted of mixed debris on coarse tephra sand, with debris coming from the vent cone to the south and rocky outcrops dominating the northern part of the valley. To the west, the valley transitioned into a broad amphitheater with smooth walls consisting of coarse tephra sand. This smooth surface ascended to a rounded ridgeline to the north, which was a sandy extension of the main summit ridge. A similar amphitheater was found at the satellite ridge crests to the east of the vent (see Figure 2b).

Volcanic Breccia (VB) was only present in a few locations in the summit area and represents fragmental material that has become cemented over time. These breccias varied greatly in terms of degree of cementation, clast size and proportion of matrix, in some cases appearing to be matrix-supported and in other cases clast-supported. They were especially distinct at Fault Shrimp, which has been a persistent area of diffuse hydrothermal venting and a long-term sampling site. Fault Shrimp itself consisted of volcanic breccia (Figure 4f), with a mantle of tephra sand that increased to the north until the ridgeline became buried in the surrounding sandy areas. The breccia was almost entirely covered in an orange-yellow alteration rind and a dense mat of microbial filaments, both related to local hydrothermal discharge. This gave the appearance of dark grey clasts spaced about 10-20 cm apart in an orange matrix, but beneath this rind the breccia were highly friable, breaking into dark, angular cm-sized clasts. Volcanic breccia was also found in outcrops along the summit ridge, where it lacked orange alteration and instead was characterized either by white sulfur covering or no covering at all. This breccia was almost entirely clast-supported, with little or no matrix evident. The clasts were angular and ranged in size from 5 to 20 cm with a mode of 20 cm.

Lava flows found at NW Rota-1 in 2009 included *Pillow Lava* (P_y, P_o) and *Sheet Flow (SF)* (Figures 4f, i, k, g). Pillow lavas were present at several locations in the summit area. In all locations the pillows had similar diameters and aspect ratios. A very distinct pile of young pillow lavas was mapped on the south side of the cone at the eruptive vent, and shows up clearly in the multibeam bathymetry (Figure 2b). These pillows were generally small and circular to tubular, ranging in diameter from 30 to 60 cm and having aspect ratios close to 1 (Figure 4g). Lobes formed closely-packed piles of tubes, with minimal intra-pillow hyaloclastite. Young pillows were also found at two other locations surrounding Brimstone vent, roughly forming a ring around the vent cone. At both locations the pillows appeared partially eroded (probably by landslide activity) and, compared to the near-vent pillows, more heavily coated in particulate sulfur (50-75% coverage). These pillow lava outcrops support the interpretation that a period of pillow lava extrusion preceded the growth of the cone of auto-brecciated debris at the vent.

Pillow lavas designated as ‘old’ (Figure 4h) were differentiated from younger ones based on year of observation, superposition, spatial distribution relative to the active eruptive vent and degree of sulfur coverage. Old pillow lavas were only found to the west of the vent, suggesting this previous phase of pillow lava emplacement was most likely covered by the products of subsequent eruptions. It is possible that this older layer of pillow lavas intermixed with tephra and breccia underlies the whole summit area.

Two areas with sheet flows were found southwest of Brimstone vent and were both located downhill from the young pillow lava flow areas. The sheet flows were often associated with the edges of pillow lava zones and the pillows appeared to transition into the sheet flows in some locations. All sheet flows exhibited some degree of surface erosion (probably as a result of subsequent landslide activity and being emplaced on a slope), but clearly had a hackly surface texture (Figure 4i). The presence of sheet flows and their association with the pillow lavas is additional evidence in support of a higher eruption rate period prior to formation of the debris cone.

5. Observations in 2010

5.1. Multibeam Bathymetry

The summit of NW Rota-1 was strikingly different in 2010 (Figure 2c) because of the major landslide that took place in August 2009, between the 2009 and 2010 expeditions [*Chadwick et al.*, 2012]. Whereas the summit landscape in both 2004 and 2009 was dominated by vent-related constructional features, the landscape in 2010 was almost completely altered by the landslide and dominated by an elevated summit platform bordered by steep cliffs. The landslide removed almost all of the previously deposited unconsolidated eruptive products from the summit. The new cliffs measured 30-60 m high, were nearly vertical in places, and surrounded the summit platform on three sides. The blocky debris cone that had grown between 2006-2009 was completely removed by the 2009 landslide, but a conical construction was still centered at the location of Brimstone vent, sitting about 30 m deeper than in 2009 (but still 10 m higher than in 2004). If this Brimstone-centered cone was a remnant of the 2009 landslide it must have been constructed of more resistant material and may well have been comprised of lavas that were extruded between 2006 and 2009. Alternately, it could have formed as a result of ultra-slow extrusion in the time between the 2009 landslide and the 2010 ROV visits, as this style of eruption was still going on intermittently at some of the vents in 2010. The Fault Shrimp ridge remained largely intact, but was significantly eroded by the landslide in its lower reaches. East and west of the summit platform, the headwall of the landslide moved the summit ridge northward by about 60-100 m (Figure 10). To the northeast of the landslide headwall, the smooth northern flank of the seamount was left largely intact.

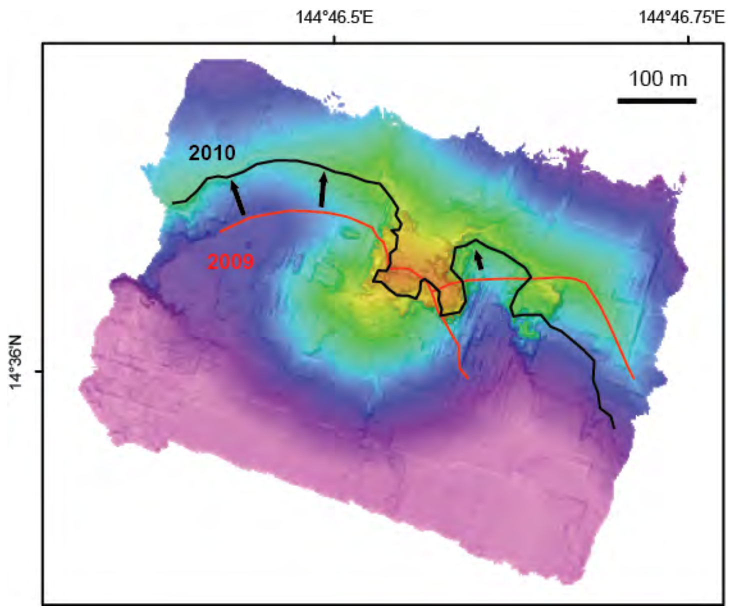

Figure 10. Location of the summit ridge in 2009 (pre-landslide, in red) and landslide headwall scarp in 2010 (post-landslide, in black), showing that the headwall scarp migrated 100 m northwards as a result of the 2009 landslide.

5.2. Depth Changes

Depth changes calculated between the 2009 and 2010 surveys show a major loss of material (Figure 2e) when compared to the previous multibeam survey in 2009, with a volume of 5.36×10^6 m^3 removed from the summit area. This is a minimum estimate, since it only includes the area of the high-resolution surveys. Depth changes over a larger area from ship-based multibeam surveys showed that a volume of 53×10^6 m^3 had been removed by the landslide [*Chadwick et al.*, 2012]. The largest depth changes at the summit (up to -93 m) were focused in two arcuate zones where the summit ridges were formerly located, to the east and west of the main summit platform. These two ridges of largely unconsolidated material were entirely removed due to the retreat of the landslide headwall. Over the eruptive vents about 30 m of material was removed between 2009 and 2010, and up to 50 m was removed southwest of the vents where the pillow lava pile was located in 2009. The ship-based multibeam sonar surveys show that the area where material was removed by the landslide extended downslope up to 3.5 km from the vents where eruptive debris had previously accumulated before 2009. That material, deposited over at least six years, was remobilized downslope by the landslide in a matter of hours [*Chadwick et al.*, 2012].

A longer-term comparison between the 2004 and 2010 high-resolution multibeam surveys (Figure 2f) shows that the negative depth changes are still large in the arcuate zones east and west of the summit platform, where the unconsolidated summit ridges were removed by the landslide, but there is surprisingly little net depth change near and downslope from the eruptive vents. This suggests that the 2004 and 2010 surveys represent an approximate "base-level" for the upper south flank, whereas conditions in 2009 reflected a temporary phase in volcanic construction due to the production and accumulation of blocky lava debris.

5.3. Eruptive Style

Another striking difference in 2010 was a change in the number of vents. Whereas Brimstone vent was the only eruptive vent in 2004, 2006, and 2009, there were multiple eruptive vents in 2010, each with a slightly different eruptive style. The five vents, named from west to east, Phantom, Sulfur, Brimstone, Styx and Charon, were spaced 21-38 m apart, and covered a total distance of 114 m in an east-west line (Figure 11). In 2010, Brimstone vent was still located at approximately the same location as in 2009 and was the central and shallowest of the five eruptive vents in 2010. All five vents were located at roughly the same depth except for Phantom and Charon, which were about 10 and 30 m deeper than the rest, respectively.

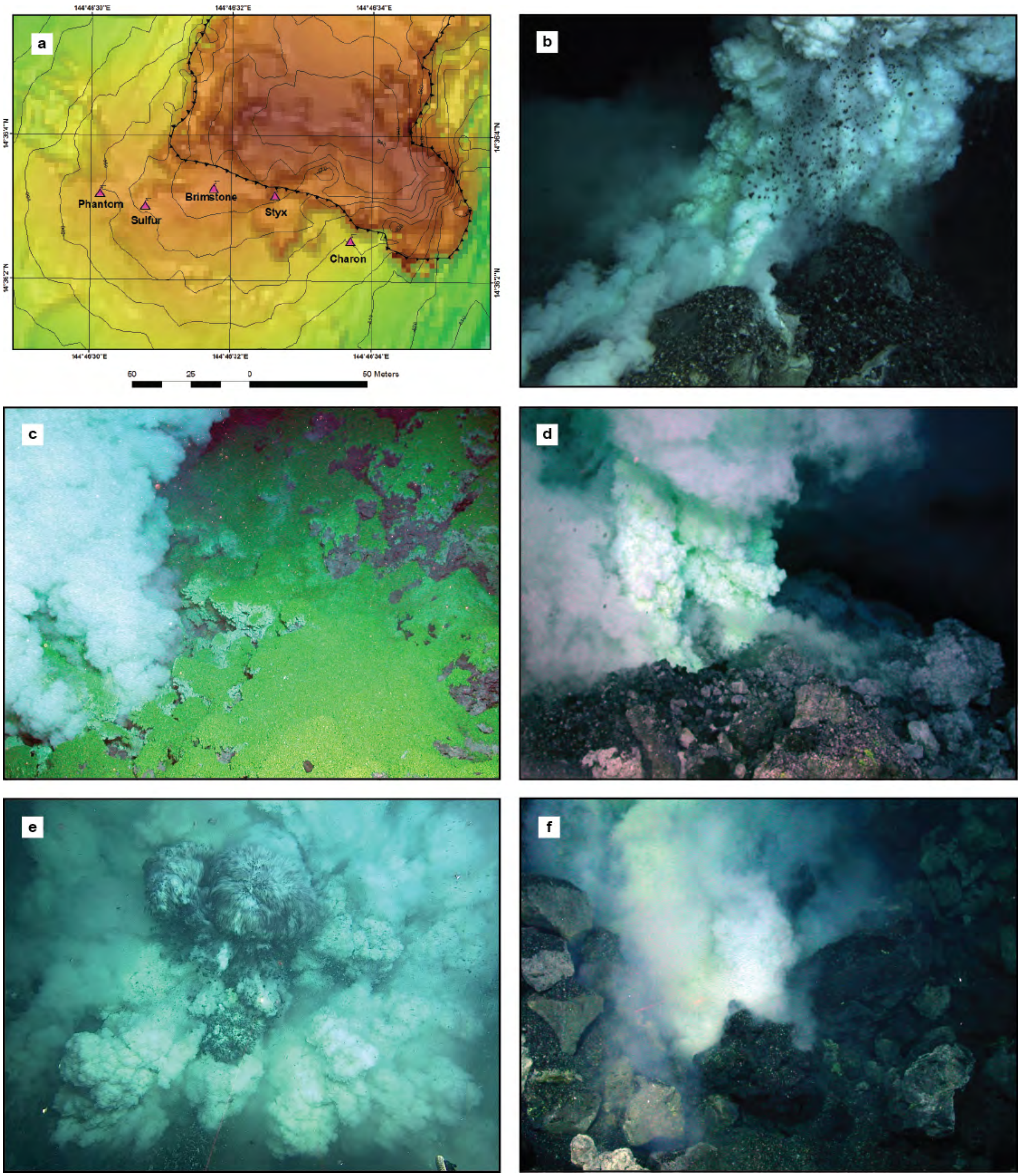

Figure 11. Eruptive vents observed in 2010. (a) Map showing linear arrangement of vents, (b) Phantom vent, (c) Sulfur vent, (d) Brimstone vent, (e) Styx vent, (f) Charon vent.

During the 2010 ROV dives, each vent started and stopped erupting independently from day-to-day and hour-to-hour [*Chadwick et al.*, 2014]. Phantom vent was characterized by large lava blocks (up to 1 m across) and coarse tephra on a steep unstable slope. Its activity alternated between explosive bursts and passive degassing (Video 6). At Sulfur vent there were extensive outcrops and deposits of tephra cemented by yellow sulfur crusts in some places, indicative of past explosive activity accompanied by discharge of molten sulfur. The activity at Sulfur vent consisted of passive degassing with occasional explosive bursts (Video 7). However, some of the (unobserved) activity must have expelled large quantities of molten sulfur droplets, because newly deposited sulfur crusts were found on the seafloor around the vent between some of the 2010 ROV dives (Figure 11c). Brimstone vent in 2010 alternated between mildly explosive activity and passive degassing and the surrounding area was a mixture of fine tephra and coarse lava blocks (Video 8). Styx vent was located in a small alcove in the cliffs at the southern edge of the summit platform. During the early visits to Styx the activity was predominantly passive degassing. Later in the expedition Styx vent hosted the most energetic explosive eruptive bursts seen in 2010, producing an extensive sheet of coarse tephra downslope (Video 9). Charon vent mostly exhibited passive degassing through a pile of angular debris on the steep slope below the summit platform cliffs (Video 10).

Relative to previous years, eruptive activity in 2010 was a mixture of the conditions in 2006 and 2009. Violent eruptive bursts featuring a churning white plume, CO_2 bubbles and abundant tephra were observed at both Styx vent and Phantom vent during 2010, similar to that observed in 2006. The other eruptive vents were characterized by more passive degassing reminiscent of activity in 2009. Styx and Sulfur vents were the main sources of CO_2 bubbles during systematic multibeam sonar surveys of the water column above the volcano in 2010 [*Chadwick et al.*, 2014]. No slow extrusion of lava spines was directly observed in 2010, but this process was likely still occurring at times as evidenced by the blocky lava debris surrounding some of the vents.

5.4. Hydrophone Observations

Hydrophone records from 2010 reveal the continuation of cyclic eruption signals, which were intermediate in amplitude between those in 2008 and 2009 (Figure 12a). Peaks in the year-long eruptive record indicate periods of higher activity, as well as the landslide that occurred in August 2009, which represents the strongest acoustic signal over the 2009-2010 period [*Chadwick et al.*, 2012]. Over the course of the 2010 expedition the acoustic amplitude fluctuated between higher values more characteristic of eruption rates observed in 2006 and lower values characteristic of the slow extrusion observed in 2009. Although a cyclicity similar to 2009 was present, the cycles were longer in duration in 2010 than in 2009. Eruptive periods lasted about 5 minutes and were separated by pauses of about 5-7 minutes (similar to the activity in 2006). The shape of the peaks was similar to those in previous years, jumping abruptly from a baseline amplitude to near the peak amplitude, then growing for several minutes before again dropping abruptly back to the baseline (Figure 12b).

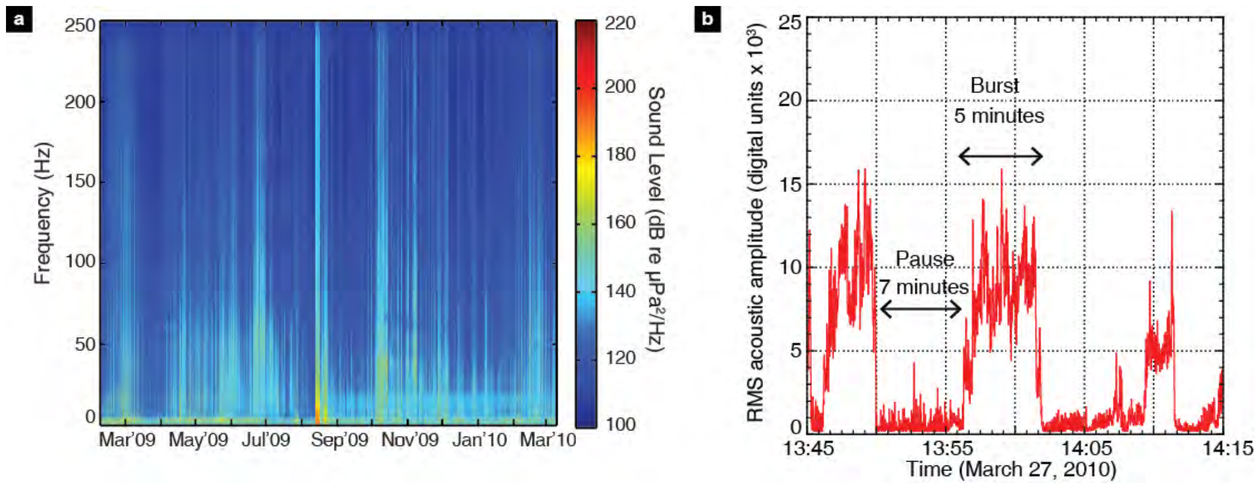

Figure 12. Hydrophone data recorded at NW Rota-1 in 2009-2010. (a) A year-long, daily average spectrogram from moored hydrophone showing sound amplitude (colors) in decibels (relative to $\mu Pa^2/Hz$) as a function of frequency versus time from February 2009 to March 2010. Vertical stripes are more or less continuous low-level Strombolian eruptive activity. The unusually large signal in middle of record is the landslide at NW Rota-1 in August 2009 (after *Chadwick et al.*, [2012]). (b) Plot of RMS acoustic amplitude (in digital units, averaged every second) measured by portable hydrophone over 30-minute time period. Portable hydrophone was deployed at the summit of NW Rota-1, and eruptive activity during this time was at Styx vent, 30 m to the south. Note the duration of eruptive periods and pauses was longer in 2010 compared to 2009, but still highly cyclical, and were intermediate in amplitude between 2008 and 2009. This hydrophone was located ~400 m from Brimstone eruptive vent.

5.5. Eruptive Deposits and 2010 Geologic Map

The post-landslide terrain of 2010 was significantly different from that observed in 2009, although areas north of the landslide headwall remained essentially unchanged (Figure 9b). The debris cone that characterized 2009 was completely removed, as were the ridges of unconsolidated material to the east and west of the summit. Blocky auto-brecciated debris was only found locally in 2010, consistent with ultra-slow lava extrusion still occurring at times and at certain vents, although much less commonly and voluminously than in 2009. This facies was found to the southwest of the summit platform at Phantom vent, which had an eruptive style most similar to that of Brimstone in 2009.

In 2010, the near-vent facies was *Outcrops and Tephra Gravel (OCT)* (Figure 4j). This facies was used to describe near-vent settings where cm-sized tephra fragments covered underlying outcrops of more consolidated material. Compared to 2009, the tephra was coarser than that found on nearby slopes and rather than blanketing the terrain evenly, it formed irregular piles relating to transport of material downslope from specific vents.

Overall, there was much more outcrop exposed in 2010 compared to 2009, which was covered in either coarse tephra sand, or coarse tephra when closer to the vents. Outcrops and coarse tephra sand was the most abundant facies in 2010 (43%) and dominated the summit platform and areas to the southwest and east, with the main summit ridge also observed in 2009 designated as undifferentiated eroded outcrop. This ridge was characterized by outcrops draped lightly in coarse tephra sand, and slopes that dropped off sharply to either side.

As in 2009, mixed debris on coarse tephra sand was found mostly downslope of the eruptive vent, but was about twice as common as in 2009 (21%). In contrast, the abundance and distribution of coarse tephra sand alone was similar to that observed in 2009. It was the dominant lithology (29%) north of the landslide headwall scarp, where it formed smooth slopes lying at the angle of repose. The Fault Shrimp area was preserved in a structurally and geologically similar condition to 2009, although it now stood out on a platform bounded by steep cliffs. The ridge, composed of volcanic breccia coated in orange microbial mat, appeared lithologically almost identical to its 2009 state.

The summit of the seamount survived the landslide, but was now surrounded by steep *Massive Flow (M)* cliffs on three sides (Figure 4k). This facies dominated the summit in 2010 and may have been partly intrusive or stock-like. These massive flows were not observed in 2009, because they had previously been buried by unconsolidated deposits, although some were likely present as undifferentiated eroded outcrops. The massive flow outcrops in 2010 had few internal structures and minimal surface alteration, indicating they had only recently been exposed. In places, these massive cliffs now marked the headwall scarp of the landslide. Figure 10 clearly shows how the summit ridge receded by 60-100 m to the north due to the landslide. The 2009 summit ridge is identified by the presence of coarse tephra sand slopes whereas the 2010 headwall scarp is delineated by the massive flow cliffs. These steep cliffs tended to transition laterally into broad areas of coarse tephra sand and outcrops and coarse tephra sand. It was not possible to identify the lava flow type forming the outcrops in the latter lithofacies, but it seems likely these were also massive flows. This suggests the massive flow cliffs may have actually extended much further around the summit bowl than currently exposed.

There was a noticeable lack of effusive lithologies (pillow lavas, sheet flows) in 2010, in contrast with 2009, where these facies were relatively abundant. The 2010 high-resolution multibeam clearly shows that the young pillow pile identified south of the vent in 2009 had been removed by the landslide. This shows the power of the 2009 landslide, which swept away lithologies generally considered resistant. However, sheet flows were identified far south of the vents in 2010, beyond the range of geologic mapping. This indicates that such lithologies are indeed present, and some have resisted removal by landslide material from above,thus becoming preserved beneath successive landslide and eruptive deposits.

6. Observations in 2014

One *JASON* ROV dive at NW Rota-1 (J2-800) was conducted during expedition RR1413 on *R/V Revelle* in December 2014, almost five years after the last observations made in 2010. Ship-based multibeam bathymetry collected in 2014 showed no significant depth changes from the previous survey in 2010, indicating that eruptive activity at NW Rota-1 had probably ceased soon after the last ROV dives in March 2010. During the 2014 ROV dive, no eruptive activity was observed, but small new pillow lava flows were found near Phantom and Charon vents (Video 11), suggesting they were produced during the final stages of eruptive activity. All the previous eruptive vents were hydrothermally active, with some emitting very passive milky plumes but none were the source of more energetic degassing associated with eruptive activity in 2009 and 2010 (Video 12). With the end of eruptive activity, hydrothermal venting had decreased in some areas, like Fault Shrimp. In other areas, the resident chemosynthetic biological community had significantly expanded, particularly near the eruptive vents which were previously too unstable and hostile. The lithofacies mapped in 2014 were very similar to those recorded in 2010, and no significant geologic changes were observed. Together, these observations suggest that no major eruptive activity or landslides occurred between 2010 and 2014.

7. Discussion

Geologic maps of the summit of NW Rota-1 reveal a clear relationship between eruptive style and lithofacies type and distribution, reflecting differences in the behavior of the volcano between 2009 and 2010. Our maps provide valuable information for assembling a comprehensive volcanic timeline spanning a decade of eruptive activity and geologic evolution at the summit of NW Rota-1 (Figure 13). In this section, we discuss the implications of these findings with respect to contrasting styles of eruption, mass wasting and edifice evolution at intra-plate and arc settings.

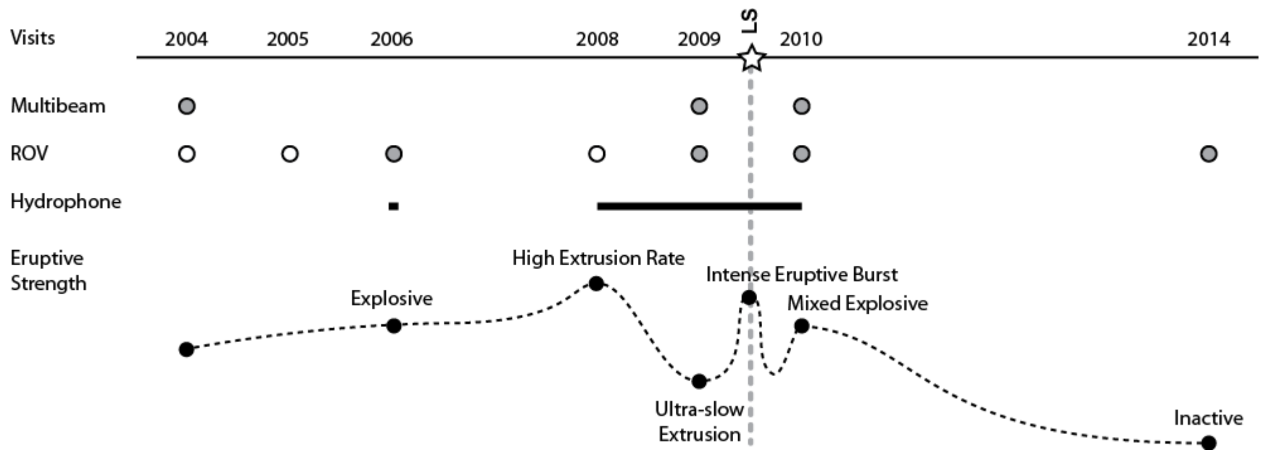

Figure 13. Timeline of observations at NW Rota-1 highlighting the data available for construction of a history of volcanic evolution, including multibeam bathymetry, ROV observations, and hydrophone recordings. Filled circles indicate data sources used in this study. Qualitative changes in relative eruptive strength are shown as an indicator of distinct temporal changes in the activity of NW Rota-1 over this 10-year time period.

7.1. Changes in Summit Geology 2004-2014

The type and distribution of lithofacies at the summit of NW Rota-1 changed considerably between 2004 and 2014. These changes are primarily a result of landslide activity, and secondarily a result of changes in eruptive style. Initial ROV observations in 2004, 2005 and 2006 showed the cyclic build-up and collapse of a cinder cone surrounding Brimstone vent, consisting of blocks and lapilli generated by relatively high-energy explosive eruptions. Then major changes occurred between 2009 and 2010, as highlighted by our geologic maps. The area near and downslope of the eruptive vent(s) and along the headwall scarp experienced the greatest changes whereas the northeastern, southeastern and northwestern slopes remained fairly similar between the two years. In 2009 the cinder cone observed in 2006 had become covered by a pile of auto-brecciated blocky lava debris which also extended downslope, covering a significant portion of the summit and upper flanks of the volcano. In 2010 this debris cone had been removed and subsequently replaced by coarse tephra overlying previously buried lava flow outcrops. The most recent observations (2014), revealed a geologic landscape mostly unaltered from 2010, due to the cessation of eruptive activity at NW Rota-1.

Of particular significance is the abundance of coarse tephra sand in all years covered by this study. This lithofacies is present both as a thin blanket over rock outcrops and as a much thicker unit on the upper flanks of the seamount (especially north of the summit), where it forms widespread smooth slopes lying at the angle of repose. The predominance of this facies indicates that NW Rota-1 has at times in the recent past experienced extended periods during which the volcano erupted large amounts of sand-sized tephra. This material would also need to be carried high enough into the water column for it to spread out and be deposited over a relatively wide area (≥ 500 m from the vent), including the summit and upper flank areas. Barreyre et al. [2011] show that a median blocky clast (D=1mm) would be dispersed more than 500 m from the vent if carried by an energetic plume reaching a height of 1200 m. At NW Rota-1 such a plume would reach the ocean surface and would then spread out laterally, permitting even greater dispersal by surface currents. The sort of energetic eruptive activity necessary to produce this sandy material and generate such a significant plume was not witnessed during the 2004-2014 ROV dives, but may have accompanied eruptive periods of higher magnitude recorded by the hydrophone in early 2008 (Figure 8a), consistent with data from a co-located turbidity sensor [*Dziak et al.*, 2012]. This tephra was also found to be more vesicular and less crystalline than material collected around the vent in 2006 and 2009, supporting the concept that this material may have originated during the higher energy eruptive activity in 2008.

The ROV dives in 2010 provide an important window into how lithology controls which parts of the volcano will are most stable and which eruptive products are susceptible to mass wasting . The majority of the unconsolidated material present around the summit in 2009 was removed by the landslide (0.53 km^3), leaving behind only resistant outcrops, pillowed and massive lava flows and consolidated volcanic breccia. These differences between facies preservation suggest a process of periodic cone build-up and downslope cascading of debris, followed by less frequent but larger landslide events during which most unconsolidated material is removed from the summit area and transported downslope. What remains is the solid core of the volcano, which is composed of both extrusive and intrusive material and may also include volcanic breccia, if it is sufficiently well cemented to avoid removal. The massive lava flow cliffs exposed in 2010 most likely represent this volcanic throat and could have been emplaced either as an intrusive stock, or as a result of the pooling of thick lava flows in a summit depression. The distribution of the older outcrops around the summit cone indicate that a large pillowed flow was emplaced at the summit before the current vent system developed, and that the younger pillows were emplaced over the underlying older base. Lava flows and intrusive bodies therefore seem to form a skeletal framework for other deposits, and have a much better chance of being stable additions to the seamount on long timescales.

The preservation of breccias at Fault Shrimp indicates that loose material must have become cemented quickly enough to avoid removal by periodic landslides. This may have been a result of high sulfur output from the eruptive vent(s), remobilization of subsurface sulfur deposits by hydrothermal activity, or the ridge could have formed during an interval of years or decades when no major landslides occurred. Given that breccias are a relatively uncommon lithofacies at the summit of NW Rota-1, this may indicate that long periods of inactivity have been relatively infrequent in the recent history of the volcano.

7.2. Changes in Eruptive Style from 2004-2014

Eruptive activity at NW Rota-1 has generally been characterized as Strombolian [*Chadwick et al.*, 2008a], although eruptive strength has varied markedly over time. During highly active periods, eruptions at NW Rota-1 are driven by high gas flux and low volume lava extrusion. However, eruptive style varied significantly between 2004 and 2014 (Figure 13). During 2004, eruptive activity was primarily gas driven, producing abundant pyroclastic debris (ash, lapilli). Eruptions were focused at a single vent, hidden from sight within a crater. In 2005 and 2006 material from the eruptive vent had filled the crater and built a small cone. The eruptive style was similar to that in 2004 but more explosive, with more efficient magma fragmentation and ejection of larger amounts of pyroclasts, including bombs.. An interlude of even higher eruption rates is suggested by the 2008-2009 hydrophone data (unobserved by ROV). NW Rota-1 then transitioned into a more sluggish eruptive period. 2009 was dominated by passive degassing and ultra-slow extrusion and auto-brecciation of lava at the vent. The periodic shaking, crumbling and extended periods of ultra-slow extrusion of lava spines were the only indicators that NW Rota-1 was still actively erupting. A brief period of intense eruptive activity accompanied or triggered the August 2009 landslide [*Chadwick et al.*, 2012]. In 2010 a partial return to the high eruptive energy of

2006 was observed, but activity died down soon thereafter and NW Rota-1 eventually became quiescent some time prior to 2014.

A major difference between 2009 and 2010 was the change from a single eruptive style at a single vent, to a system of five vents all with their own on/off timing, eruptive styles and associated deposits. The reason for this is not clear. The E-W linear arrangement and close spacing of vents centered on Brimstone in 2010 suggests that the main conduit below Brimstone was still present but had been disrupted and perhaps ruptured during the 2009 landslide event. We suspect that north-south extensional stresses in the headwall area resulting from the landslide may have allowed satellite vents to flare from the deeper, probably cylindrical, main conduit, either as separate pipes or perhaps as separate vents above a short dike-like shallow intrusion. Regardless, the intermittent and variable behavior of the eruptive vents in 2010 suggests that the shallow part of the conduit system was still being reorganized in the aftermath of the 2009 landslide.

The observations made during 2009-2010 show that eruption rate is a major control on eruptive products at submarine volcanoes. When the eruption rate is relatively high, a large volume of material is pushed to the surface, probably driven by more rapid degassing, producing lava flows and perhaps more tephra. At lower extrusion rates, magma is more likely to solidify and stall in and around the vent, allowing more rapid cooling and blocking further magma ascent for a time. Renewed slow extrusion leads to increased degassing and auto-brecciation of slowly extruded lava at the vent. At NW Rota-1 the eruption rate varied by many orders of magnitude over a decade of activity (2004-2014). Despite this variation in eruptive style over time, the eruptive activity was remarkably cyclic at multiple time scales. This suggests that the same basic mechanism is probably responsible for the cyclic behavior observed in all years when NW Rota-1 was visited and during the two year-long hydrophone deployments between 2008 and 2010. These cycles reflect a basic eruptive system of rapid quenching of lava, which clogs the vent, followed by pressure build-up of gasses beneath the chilled vent cap, and finally disruption or destruction of the cap by the rapid release of gases, resulting in explosions or extrusions. For submarine eruptions driven by magmatic degassing, temporally cyclic behavior appears to be a fundamental characteristic at a wide range of extrusion rates.

7.3. Comparison with Subaerial Eruptive Behavior

Subaerial and submarine eruptions are often thought of in very different terms due to the sharp contrast between quench conditions in air and water. This difference controls the morphologies and physical properties of eruptive products. However, there are some surprising similarities between subaerial activity and the submarine eruptive behavior at NW Rota-1. One example of this is the growth of lava spines, which were observed emerging from the vent at NW Rota-1 during the ultra-slow extrusion phase of volcanic activity during 2009. In a review of lava spine growth conditions at more silicic subaerial volcanoes, *Cashman et al.*, [2008] reported emergence rates of 3-6 m/day (Mt. St. Helens), < 25 m/day (Mont Pelée) and < 40 m/day (Unzen). This range (3-40 m/day) is surprisingly similar to rates of 24-144 m/day estimated from time-lapse videos at NW-Rota-1, despite the difference in lava composition (dacite at the subaerial volcanoes and basaltic andesite at NW Rota-1). Of course, the volumetric effusion rates are quite different since the eruptive vent at NW Rota-1 has such a small cross-sectional area compared to these subaerial examples. Nevertheless, these similarities in spine-growth velocities suggest that the ascent (decompression) rate controlling syn-ascent crystallization (rheology) and degassing is fairly similar in all these cases, and may control volcanic eruption styles in these two different environments.

7.4. Long-Term Edifice Evolution at Submarine Volcanoes

Submarine volcanoes evolve from simple pillow mounds just a few hundred meters high, to complex, unstable edifices several kilometers in height [*Schnur and Gilbert*, 2012; *Staudigel and Schmincke*, 1984]. Seamount growth is driven both by extrusive emplacement of lava flows and by the build-up of unconsolidated fragmental material. Once a height and slope threshold of instability is reached, these edifices begin to disaggregate in the form of small-scale creep, episodic landsliding, and major sector collapse. Our knowledge of seamount evolution has been largely based on ocean-island volcanoes with subaerial portions and unstable flanks, such as Hawaii, the Canary Islands, and Tristan da Cunha [*Caratori Tontini et al.*, 2013; *Holcomb and Searle*, 1991; *Krastel et al.*, 2001; *Mitchell*, 2002, 2003; *Moore et al.*, 1994], and more recently on arc-related volcanic islands such as Montserrat and other sites in the Lesser Antilles [e.g. Coussens et al. 2015, le Friant et al. 2015, Watt et al 2015]. The repetitive growth and collapse of smaller, completely submarine arc volcanoes is more poorly studied. This distinction is important because tectonic setting has a major impact on the nature of seamount growth and collapse. This setting modulates the rheology of magmas and therefore the explosivity of eruptions, as well as the rate and volume of magma supply, which determine the frequency and size of eruptions as well as landslide events. The submarine environment contributes to these differences in that submarine volcanoes tend to be smaller, generating smaller landslides, and the rapid cooling of material is more likely to produce fragmental eruptive products rather than coherent lithologies.

Constructive and destructive processes have been documented at several active submarine arc volcanoes, of which only a few other than NW Rota-1 have been particularly well-studied. West Mata, a volcano in the NE Lau basin, is the only seamount other than NW Rota-1 where active submarine eruptions have been directly observed from an ROV [*Resing et al.*, 2011]. Similar to NW Rota-1, West Mata is roughly conical with smooth slopes broken only by rift zones, although its summit is much deeper (1159 m) and the volume of the edifice is much smaller (~26.6 km^3) [*Clague et al.*, 2011]. Eruptive activity observed in 2009 at West Mata was much more vigorous than that observed at NW Rota-1, including explosive degassing, pillow lava flows and vigorous ejection of pyroclasts [*Dziak et al.*, 2015; *Resing et al.*, 2011]. Like at NW Rota-1, West Mata was apparently continuously active for at least several years erupting from multiple vents, experienced multiple landslide events, and then became inactive in 2011 [*Bohnenstiehl et al.*, 2014; *Caplan-Auerbach et al.*, 2014; *Embley et al.*, 2014].

Monowai Cone is one of the most volcanically active submarine volcanoes in the Kermadec Arc and is located on the southern margin of the larger (10 km long) Monowai Caldera. The cone is about 10 -12 km in diameter, and rises over 1400 m to a depth of about 130 m [*Graham et al.*, 2008]. For decades, remote detection from land-based seismic monitoring in Polynesia [*Talandier and Okal*, 1987, 2001] and distant hydrophones [*Metz et al.*, 2016], combined with visual surveillance made by fly overs [e.g. *Davey*, 1980], has detected intermittent eruptive activity at Monowai, sometimes accompanied by the presence of discolored water at the ocean surface and extensive bubbles of CO_2 streaming through the water column (CEJ de Ronde, pers. Obs., 2002). Most recently, knowledge of Monowai's activity comes from repeated bathymetric surveys, which have shown successive build-up and landsliding of individual sectors of the cone [*Chadwick et al.*, 2008b; *Watts et al.*, 2012; *Wright et al.*, 2008].

Similar to NW Rota-1, both West Mata and Monowai have experienced cyclic construction and destruction and repeat bathymetric surveys have revealed positive and negative depth changes of tens of meters (sometimes >100 m) over just a few years. The smooth slopes of these volcanoes mainly consist of clastic volcanic debris, resulting in distinct conical edifices. Headwall scarps of larger landslides and mass wasting tongues have been mapped at the summits and lower flanks of all three volcanoes. The cyclicity of the reconstruction at these volcanoes is therefore a result of the periodic build-up and collapse of fragmental material due to landslides.

Possible landslide triggers include oversteepening of debris piles due to eruptive activity, intrusion-related expansion, weakening of deposits in hydrothermal upflow zones, loading of gravitationally unstable substrate, and volcanic or tectonically-related seismic activity [*Chadwick et al.*, 2008b]. Of these, eruption-related oversteepening likely results in periodic shedding of small amounts of material at smaller seamounts. The estimated threshold elevation of instability for seamounts is about 2.5 km, after which slope steepening and an increasing proportion of volcaniclastic material makes sector collapse more likely [*Mitchell*, 2001]. Weakening of initiation zones by hydrothermal alteration is another possible driver of instability [e.g. *McGuire*, 2016], although hydrothermal fluid can also play a role in cementation and strengthening due to palagonitization. There appears to be a weak correlation with hydrothermal upflow zones at NW

Rota-1 and the source area of landslide events. At Monowai, the headwall scarp of a major landslide coincided with pre-collapse areas of hydrothermal venting [*Wright et al.*, 2008]. *Caratori Tontini et al.*, [2013] hypothesize that the weakening of flanks by hydrothermal alteration may have precipitated collapse at Rumble III volcano in the Kermadec Arc. At nearby Clark volcano, current-day hydrothermal activity is associated with the heads of some sector collapse scarps [*de Ronde et al.*, 2014]. These examples indicate that hydrothermal fluids most likely play an important role in destructive processes at arc volcanoes.

Seismic activity may also be energetic enough to trigger major landslides. *Chadwick et al.* [2012] show that in the case of NW Rota-1, the 2009 landslide was triggered by a seismic swarm and volcanic eruption. Coussens et al. [2015] show a link between periods of volcanic activity at Montserrat and increased volcano instability, in the form of landslides. It therefore seems likely that eruptions, perhaps with a minimum intensity threshold, are a strong triggering mechanism for slope collapse, but that hydrothermal activity contributes to weakening slopes, increasing the likelihood of sector or flank collapse. In any case, the size and frequency of landslide events appears to be directly related to the magnitude and frequency of eruptive activity and the volume of loose eruptive products deposited on the upper volcano slopes.

Larger intra-plate edifices (e.g. Hawaii, La Réunion, Tristan da Cunha, Canary Islands, American Samoa, St. Helena [*Holcomb and Searle*, 1991]) experience more catastrophic but much less frequent landslides, which may have more complex histories and initiating mechanisms. This distinction may be a result of the internal structure of these islands and seamounts and is probably also related to the relative frequency of explosive eruptions in the two settings. Whereas andesitic arc volcanoes tend to produce large volumes of tephra, resulting in steep slopes of unconsolidated debris, basaltic intra-plate submarine volcanoes are more likely to be composed of solid lithologies. Their internal structure consists mostly of pillow lavas, sheet flows and massive flows interspersed with volcanic breccia, later cut by intrusions and sills [*Schnur and Gilbert*, 2012; *Staudigel and Schmincke*, 1984]. They are therefore less prone to episodic slides, but when fracturing occurs along planes of weakness resulting from hydrothermal activity, the volcano is more likely to release a large intact block of consolidated material, leaving behind obvious slumps and large block deposits at the base of the volcano.

These relationships are broadly supported by recent detailed work at Montserrat arc volcano. Coussens et al. [2015] found that mass-wasting events at Montserrat were roughly associated with periods of rapid global sea-level rise for arc volcanoes, but not for intra-plate volcanoes. They proposed a similar explanation relating the more lithologically diverse flanks of arc volcanoes to their greater susceptibility to mass wasting. However, blocks from large sector collapse events have been observed below sea level at Montserrat, the largest of which is composed of volcanic breccia [Watt et al. 2015]. Therefore large-scale sector collapse is indeed possible at arc volcanoes, most likely in cases where volcanic breccias are abundant and well-consolidated.

By contrasting submarine arc volcanoes and intra-plate seamounts we can consider their mass wasting frequency and landslide volumes as opposite ends of a spectrum. The volume of the landslide at NW Rota-1 in 2009 is similar to landslides at other arc volcanoes but small compared to those recorded at larger intra-plate edifices. Monowai experienced two slides between 1998 and 2007 with volumes of 0.040 and 0.085 km^3 [*Chadwick et al.*, 2008b]. West Mata also experienced a landslide with a relatively small estimated volume of 0.076 km^3 [*Clague et al.*, 2011; *Embley et al.*, 2014]. In comparison, the volume of the 2009 NW Rota-1 landslide was estimated at 0.034 km^3, the same order of magnitude to those recorded at Monowai and West Mata.

The volumes of these small landslides are almost insignificant compared to larger slides due to sector collapse such as the Mount St. Helens debris avalanche (2 km^3) , numerous Hawaiian landslides and slumps (10s-1000s of km^3) [*Holcomb and Searle*, 1991, Moore et al. 1994], and the landslides of the Canary Islands (25-1000 km^3) [Krastel et al. 2001]. Compared to the volume of the NW Rota-1 volcanic cone (134 km^3) the 2009 landslide represents less than 0.1% of the total edifice. At larger intra-plate volcanoes, single landslides can remove up to 10-20% of the whole edifice [*Holcomb and Searle*, 1991]. The volume of the NW Rota-1 landslide is also relatively small when compared to the volume of other volcanic debris avalanches. These range from about 0.1 to 10 km^3 in a compilation of size metrics from 43 avalanche deposits, based on subaerial volcanoes [*Ui*, 1983]. At Montserrat, similarly large debris avalanche volumes of up to 20 km^3 have been estimated based on submarine deposits [Lebas et al. 2011]. Deposits of greater than 250 km^3 are estimated at Martinique [le Friant et al. 2015], although such deposits may often contain a significant proportion of hemipelagic sediment [e.g. Watt et al. 2012].

The timing and frequency of ancient landslides is less well constrained. NW Rota-1 has been studied for only ten years, during which time one landslide occurred. Gaps between eruptive periods at sites in the Lesser Antilles ranged from tens to hundreds of thousands of years [le

Friant et al. 2015, Coussens et al. 2015, Watt et al. 2012]. The study of older landslides is limited in areas of high sedimentation, but large slides as old as 15 Ma have been identified off the Canary Islands [Krastel et al. 2001], suggesting gaps of hundreds of thousands of years up to millions of years between major events. In the Hawaiian Islands, the largest landslides occur during the late shield-building stage of volcano formation, and therefore mirror the age progression of the island chain. Based on this rough dating method, Moore et al. [1994] estimate the frequency of major landslides at one every 350 ka. We therefore suggest that intra-plate volcanoes represent the large volume – low frequency end of a seamount mass wasting spectrum, with small submarine arc volcanoes such as NW Rota-1 forming the low volume – high frequency end of this range and subaerial arc volcanoes falling in the middle of the spectrum

There is a complex relationship between eruptive style, eruptive products, and the long-term construction and destruction of volcanic edifices. Observations at actively erupting submarine arc volcanoes suggest that constructive and destructive processes are interrelated, repetitive and possibly cyclical, reflecting the underlying cyclical nature of eruptive processes at subduction zone settings. The more viscous lavas erupted at arcs result in explosive eruptions and the production of unconsolidated tephra deposits whereas intra-plate settings tend to be dominated by lower-silica magmas which form effusive products. These geologic differences affect the cohesiveness of the edifice and susceptibility to mass wasting. Active arc volcanoes therefore experience frequent (10s to 100s of thousands of years) small-scale (< 1 to 10s ofkm^3) landslides likely triggered by eruptive episodes whereas intra-plate volcanoes experience less frequent (100s of thousands to millions of years) landslides, but when they do occur they are very large (100s-1000s of km^3) and are likely triggered by alteration-related or rift-zone intrusion instability.

In both cases, landslides represent a significant agent of change in the geologic history of seamounts.

Acknowledgements

This research was supported in part by a Hatfield Marine Science Center Mamie Markham Research Award to S. Schnur and National Science Foundation awards OCE-0751776 and OCE-1233717 to W. Chadwick. Additional funding for the fieldwork in 2014 was provided by NOAA Ocean Exploration and Research Program award OE_FY14_71. We thank the captains and crews of R/V *Thompson* (Cruise TN-232 in 2009), R/V *Kilo Moana* (Cruise KM-1005 in 2010), and R/V *Revelle* (Cruise RR1413 in 2014), and the *JASON* ROV teams on all three expeditions. Data and reports from the cruises above are available on-line at the IEDA Marine Geoscience Data System (http://www.marine-geo.org/index.php). PMEL contribution number 4585.

References

Baker, E. T., R. W. Embley, S. L. Walker, J. a. Resing, J. E. Lupton, K. Nakamura, C. E. J. de Ronde, and G. J. Massoth (2008), Hydrothermal activity and volcano distribution along the Mariana arc, *Journal of Geophysical Research*, *113*(B8), B08S09, doi:10.1029/2007JB005423.

Bohnenstiehl, D. R., R. P. Dziak, H. Matsumoto, and J. A. Conder (2014), Acoustic response of submarine volcanoes in the Tofua Arc and northern Lau Basin to two great earthquakes, *Geophysical Journal International*, *196*, 1657–1675, doi:10.1093/gji/ggt472.

Butterfield, D. A., K. Nakamura, B. Takano, M. D. Lilley, J. E. Lupton, J. A. Resing, and K. K. Roe (2011), High SO2 flux, sulfur accumulation, and gas fractionation at an erupting submarine volcano, *Geology*, *39*(9), 803–806, doi:10.1130/G31901.1.

Caplan-Auerbach, J., R. P. Dziak, D. R. Bohnenstiehl, W. W. Chadwick, and T. Lau (2014), Hydroacoustic investigation of submarine landslides, *Geophysical Research Letters*, *41*, 5927–5934, doi:10.1002/2014GL060964.

Caratori Tontini, F., C. E. J. de Ronde, J. C. Kinsey, A. Soule, D. Yoerger, and L. Cocchi (2013), Geophysical modeling of collapse-prone zones at Rumble III seamount, southern Pacific Ocean, New Zealand, *Geochemistry, Geophysics, Geosystems*, *14*(10), 4667–4680, doi:10.1002/ggge.20278.

Cashman, K. V, C. Thornber, and J. S. Pallister (2008), From Dome to Dust: Shallow Crystallization and Fragmentation of Conduit Magma During the 2004 – 2006 Dome Extrusion of Mount St . Helens , Washington, in *A Volcano Rekindled: The Renewed Eruption of Mount St. Helens, 2004-2006*, edited by D. Sherrod, W. Scott, and P. Stauffer, pp. 387–413.

Chadwick, W. W., K. V. Cashman, R. W. Embley, H. Matsumoto, R. P. Dziak, C. E. J. de Ronde, T. K. Lau, N. D. Deardorff, and S. G. Merle (2008a), Direct video and hydrophone observations of submarine explosive eruptions at NW Rota-1 volcano, Mariana arc, *Journal of Geophysical Research*, *113*(B08S10), 1–23, doi:10.1029/2007JB005215.

Chadwick, W. W., R. P. Dziak, J. H. Haxel, R. W. Embley, and H. Matsumoto (2012), Submarine landslide triggered by volcanic eruption recorded by in situ hydrophone, *Geology*, *40*(1), 51–54, doi:10.1130/G32495.1.

Chadwick, W. W., S. G. Merle, N. J. Buck, J. W. Lavelle, J. A. Resing, and V. Ferrini (2014), Imaging of CO2 bubble plumes above an erupting submarine volcano, NW Rota-1, Mariana Arc, *Geochemistry Geophysics Geosystems*, *15*, 4325–4342, doi:10.1002/2014GC005543.

Chadwick, W. W., D. S. Scheirer, R. W. Embley, and H. P. Johnson (2001), High-resolution bathymetric surveys using scanning sonars: Lava flow morphology , hydrothermal vents , and geologic structure at recent eruption sites on the Juan de Fuca Ridge, *Journal of*

Geophysical Research, *106*(B8), 16075–16099.

Chadwick, W. W., I. C. Wright, U. Schwarz-Schampera, O. Hyvernaud, D. Reymond, and C. E. J. de Ronde (2008b), Cyclic eruptions and sector collapses at Monowai submarine volcano, Kermadec arc: 1998-2007, *Geochemistry, Geophysics, Geosystems*, *9*(10), doi:10.1029/2008GC002113.

Clague, D. A., J. B. Paduan, D. W. Caress, H. Thomas, W. W. C. Jr, and S. G. Merle (2011), Volcanic morphology of West Mata Volcano, NE Lau Basin, based on high-resolution bathymetry and depth changes, *Geochemistry, Geophysics, Geosystems*, *12*(11), 1–21, doi:10.1029/2011GC003791.

Davey, F. (1980), The Monowai seamount: an active submarine volcanic centre on the Tonga-Kermadec ridge (Note), *New Zealand Journal of Geology and Geophysics*, *23*(4), 533–536, doi:10.1080/00288306.1980.10424124.

Deardorff, N. D., K. V. Cashman, and W. W. Chadwick (2011), Observations of eruptive plume dynamics and pyroclastic deposits from submarine explosive eruptions at NW Rota-1, Mariana arc, *Journal of Volcanology and Geothermal Research*, *202*(1–2), 47–59, doi:10.1016/j.jvolgeores.2011.01.003.

Dziak, R. P., E. T. Baker, a. M. Shaw, D. R. Bohnenstiehl, W. W. Chadwick, J. H. Haxel, H. Matsumoto, and S. L. Walker (2012), Flux measurements of explosive degassing using a yearlong hydroacoustic record at an erupting submarine volcano, *Geochemistry, Geophysics, Geosystems*, *13*(11), doi:10.1029/2012GC004211.

Dziak, R. P., D. R. Bohnenstiehl, E. T. Baker, H. Matsumoto, J. Caplan-Auerbach, R. W. Embley, S. G. Merle, S. L. Walker, T. K. Lau, and W. W. Chadwick (2015), Long-term explosive degassing and debris flow activity at West Mata submarine volcano, *Geophysical*

Research Letters, *42*(5), 1480–1487, doi:10.1002/2014GL062603.

Embley, R. W. et al. (2006), Long-term eruptive activity at a submarine arc volcano, *Nature*, *441*(7092), 494–7, doi:10.1038/nature04762.

Embley, R. W. et al. (2014), Eruptive modes and hiatus of volcanism at West Mata seamount, NE Lau basin: 1996-2012, *Geochemistry, Geophysics, Geosystems*, *15*, 4093–4115, doi:10.1002/2014GC005387.Received.

Embley, R. W., E. T. Baker, W. W. Chadwick, J. E. Lupton, J. A. Resing, G. J. Massoth, and K. Nakamura (2004), Explorations of Mariana Arc volcanoes reveal new hydrothermal systems, *Eos, Transactions American Geophysical Union*, *85*(4), 37, doi:10.1029/2004EO040001.

Ferrini, V. L., M. K. Tivey, S. M. Carbotte, and F. Martinez (2008), Variable morphologic expression of volcanic, tectonic, and hydrothermal processes at six hydrothermal vent fields in the Lau back-arc basin, *Geochemistry, Geophysics, Geosystems*, *9*(7), doi:10.1029/2008GC002047.

Graham, I. J., A. G. Reyes, I. C. Wright, K. M. Peckett, I. E. M. Smith, and R. J. Arculus (2008), Structure and petrology of newly discovered volcanic centers in the northern Kermadec-southern Tofua arc, South Pacific Ocean, *Journal of Geophysical Research: Solid Earth*, *113*(8), doi:10.1029/2007JB005453.

Hanson, M., S. Beaulieu, V. Tunnicliffe, J. W. W. Chadwick, and E. Breuer (2015), Looking for larvae above an erupting submarine volcano, NW Rota-1, Mariana arc, Abstract OS43A-2029 presented at 2015 Fall Meeting, AGU, San Francisco, California, 14-18 Dec.

Holcomb, R. T., and R. C. Searle (1991), Large landslides from oceanic volcanoes, *Marine Geotechnology*, *10*, 19–32, doi:10.1080/10641199109379880.

Krastel, S., H. Schmincke, C. L. Jacobs, R. Rihm, T. P. Le Bas, and B. Alibes (2001), Submarine landslides around the Canary Islands, *Journal of Geophysical Research*, *106*(B3), 3977–3997.

Limén, H., S. K. Juniper, V. Tunnicliffe, and M. Clément (2006), Benthic community structure on two peaks of an erupting seamount: Northwest Rota-1 Volcano, Mariana Arc, western Pacific, *Cahiers de Biologie Marine*, *47*(4), 457–463.

Lupton, J. E., M. Lilley, D. Butterfield, L. Evans, R. W. Embley, G. Massoth, B. Christenson, K. I. Nakamura, and M. Schmidt (2008), Venting of a separate CO2-rich gas phase from submarine arc volcanoes: Examples from the Mariana and Tonga-Kermadec arcs, *Journal of Geophysical Research: Solid Earth*, *113*(8), doi:10.1029/2007JB005467.

McGuire, W. J. (2016), Lateral collapse and tsunamigenic potential of marine volcanoes, in *Mechanisms of Activity and Unrest at Large Calderas*, vol. 269, edited by C. Troise, G. De Natale, and S. R. J. Kilburn, pp. 121–140, The Geological Society of London.

Metz, D., A. B. Watts, I. Grevemeyer, M. Rodgers, and M. Paulatto (2016), Ultra-long-range hydroacoustic observations of submarine volcanic activity at Monowai, Kermadec Arc, *Geophysical Research Letters*, *43*(4), 1529–1536, doi:10.1002/2015GL067259.

Meyer, J. L., and J. A. Huber (2014), Strain-level genomic variation in natural populations of Lebetimonas from an erupting deep-sea volcano., *The ISME journal*, *8*(4), 867–80, doi:10.1038/ismej.2013.206.

Mitchell, N. (2002), The morphology of the submarine flanks of volcanic ocean islands A comparative study of the Canary and Hawaiian hotspot islands, *Journal of Volcanology and Geothermal Research*, *115*(1–2), 83–107, doi:10.1016/S0377-0273(01)00310-9. [online] Available from: http://linkinghub.elsevier.com/retrieve/pii/S0377027301003109

Mitchell, N. C. (2001), Transition from circular to stellate forms of submarine volcanoes, *Journal of Geophysical Research*, *106*(B2), 1987–2003.

Mitchell, N. C. (2003), Susceptibility of mid-ocean ridge volcanic islands and seamounts to large-scale landsliding, *Journal of Geophysical Research*, *108*(B8), doi:10.1029/2002JB001997.

Moore, J. G., W. R. Normark, and R. T. Holcomb (1994), Giant Hawaiian Landslides, *Annual Review of Earth and Planetary Sciences*, *22*, 119–144.

Resing, J. A. et al. (2011), Active submarine eruption of boninite in the northeastern Lau Basin, *Nature Geoscience*, *4*(11), 799–806, doi:10.1038/ngeo1275.

Resing, J. a., E. T. Baker, J. E. Lupton, S. L. Walker, D. A. Butterfield, G. J. Massoth, and K. Nakamura (2009), Chemistry of hydrothermal plumes above submarine volcanoes of the Mariana Arc, *Geochemistry, Geophysics, Geosystems*, *10*(2), doi:10.1029/2008GC002141.

Resing, J. A., G. Lebon, E. T. Baker, J. E. Lupton, R. W. Embley, G. J. Massoth, W. W. Chadwick, and C. E. J. de Ronde (2007), Venting of Acid-Sulfate Fluids in a High-Sulfidation Setting at NW Rota-1 Submarine Volcano on the Mariana Arc, *Economic Geology*, *102*, 1047–1061.

Ronde, C. E. J. de et al. (2014), The anatomy of a buried submarine hydrothermal system, Clark Volcano, Kermadec Arc, New Zealand, *Economic Geology*, *109*(8), 2261–2292, doi:10.2113/econgeo.109.8.2261.

Schnur, S. R., and L. a. Gilbert (2012), Detailed volcanostratigraphy of an accreted seamount: Implications for intraplate seamount formation, *Geochemistry, Geophysics, Geosystems*, *13*(Q0AM05), doi:10.1029/2012GC004301.

Sherrin, J., V. Tunnicliffe, and J. Taylor (2011), Temporal change in population structure and genetic diversity of alvinocarid shrimp that rapidly recolonize an actively erupting submarine volcano, Abstract presented at the World Conference on Marine Biodiversity, Aberdeen, Scotland, 26-30 September.

Staudigel, H., and H. Schmincke (1984), The Pliocene Seamount Series of La Palma/Canary Islands, *Journal of Geophysical Research*, *89*(B13), 11195–11215.

Stern, R. J., M. J. Fouch, and S. L. Klemperer (2003), An overview of the Izu-Bonin-Mariana subduction factory, in *Inside the Subduction Factory*, vol. 138, pp. 175–222.

Talandier, J., and E. A. Okal (1987), Seismic Detection of Underwater Volcanism: The Example of French Polynesia, *Pure Applied Geophysics*, *125*(6), 919–950.

Talandier, J., and E. A. Okal (2001), Identification Criteria for Sources of T Waves Recorded in French Polynesia, *Pure Applied Geophysics*, *158*, 567–603.

Tamura, Y. et al. (2011), Two Primary Basalt Magma Types from Northwest Rota-1 Volcano, Mariana Arc and its Mantle Diapir or Mantle Wedge Plume, *Journal of Petrology*, *52*(6), 1143–1183, doi:10.1093/petrology/egr022.

Ui, T. (1983), Volcanic Dry Avalanche Deposits.pdf, *Journal of Volcanology and Geothermal Research*, *18*, 135–150.

Walker, S. L., E. T. Baker, J. a. Resing, W. W. Chadwick, G. T. Lebon, J. E. Lupton, and S. G. Merle (2008), Eruption-fed particle plumes and volcaniclastic deposits at a submarine volcano: NW Rota-1, Mariana Arc, *Journal of Geophysical Research*, *113*(B8), B08S11, doi:10.1029/2007JB005441.

Watts, A. B., C. Peirce, I. Grevemeyer, M. Paulatto, W. Stratford, D. Bassett, J. A. Hunter, L. M. Kalnins, and C. E. J. de Ronde (2012), Rapid rates of growth and collapse of Monowai submarine volcano in the Kermadec Arc, *Nature Geoscience*, *5*(7), 510–515, doi:10.1038/ngeo1473.

Wright, I. C., W. W. Chadwick, C. E. J. de Ronde, D. Reymond, O. Hyvernaud, H. H. Gennerich, P. Stoffers, K. Mackay, M. a. Dunkin, and S. C. Bannister (2008), Collapse and reconstruction of Monowai submarine volcano, Kermadec arc, 1998-2004, *Journal of Geophysical Research: Solid Earth*, *113*, 1998–2004, doi:10.1029/2007JB005138.